On a Simple Empirical Parameterization of Topography-Catalyzed Diapycnal Mixing in the Abyssal Ocean

THOMAS DECLOEDT AND DOUGLAS S. LUTHER

School of Ocean and Earth Science and Technology, University of Hawaii at Manoa, Honolulu, Hawaii

(Manuscript received 24 April 2009, in final form 3 September 2009)

ABSTRACT

The global spatial distribution of the turbulent diapycnal diffusivity in the abyssal ocean is reexamined in light of the growing body of microstructure data revealing bottom-intensified turbulent mixing in regions of rough topography. A direct and nontrivial implication of the observed intensification is that the diapycnal diffusivity K_ρ, is depth dependent and patchily distributed horizontally across the world's oceans. Theoretical and observational studies show that bottom-intensified mixing is dependent upon a variety of energy sources and processes whose contributions to mixing are sufficiently complex that their physical parameterization is premature; only rudimentary parameterizations of tidally induced mixing have been attempted, although the tides likely provide no more than half of the mechanical energy available for diapycnal mixing in the abyssal ocean. Here, an empirical (and still rudimentary) parameterization of the spatially variable mean diffusivity K_ρ based on a large collection of microstructure data from several oceanic regions, is provided. The parameterization, called the roughness diffusivity model (RDM), depends only on seafloor roughness and height above bottom and has the advantage of tacitly including a broad range of mixing processes catalyzed by the roughness or acuteness of the bottom topography. The study focuses in particular on the vertical structure of K_ρ and shows that exponential decay, prominent in current diapycnal mixing parameterizations, does not provide an adequate representation of the mean vertical profile. Instead, an inverse square law decay with a scale height and maximum near-boundary value depending on topographic roughness is shown to provide a more realistic vertical structure. Resulting basin-averaged diffusivities based on the RDM, which increase from $\sim 3 \times 10^{-5}$ m^2 s^{-1} at 1-km depth to $\sim 1.5 \times 10^{-4}$ m^2 s^{-1} at 4 km, are roughly consistent with spatial averages derived from hydrographic data inversions, supporting the contention that strong, localized mixing plays a major role in maintaining the observed abyssal stratification. The power required to sustain the stratification in the abyssal ocean (defined as 40°S–48°N, 1–4-km depth) is shown to be sensitive to the spatial distribution of the mixing. The power consumption in this domain, given the parameterized bottom-intensified and horizontally heterogeneous diffusivity structure in the RDM, is estimated as approximately 0.37 TW (TW = 10^{12} W), considerably less than the canonical value of ~ 2 TW estimated under the assumption of a uniform diffusivity of $\sim 10^{-4}$ m^2 s^{-1} in the abyssal ocean.

1. Introduction and motivation

Diapycnal mixing[1] occurs at scales of decameters to millimeters where turbulence generates property gradients that are irreversibly destroyed by molecular diffusion. The physical processes leading to turbulence in the abyssal ocean (depth > 1 km) are generally associated with instabilities of the internal wave field on vertical scales of $O(10$ m) (e.g., McComas and Müller 1981; Henyey et al. 1986; Toole 1998). These scales will remain unresolved, and most of the turbulence producing physical processes will remain unincorporated, in ocean general circulation models (OGCMs), for the foreseeable future. In spite of the small scales associated with

Corresponding author address: Thomas Decloedt, Marine Sciences Bldg., 1000 Pope Rd., Honolulu, HI 96822.
E-mail: decloedt@hawaii.edu

[1] Diapycnal mixing refers to mixing across surfaces of equal density (isopycnals). Strictly speaking, we are concerned here with dianeutral mixing, that is, mixing across surfaces along which water parcels can be exchanged locally without requiring work. Because of the nonlinearity of the equation of state, isopycnal surfaces do not generally coincide with neutral surfaces. Nevertheless, in the context of ocean mixing, people usually use the terms ''vertical'' or ''diapycnal'' to mean dianeutral. Herein we will follow convention and use the term diapycnal mixing. Given the small isopycnal slopes in the abyssal ocean, these terms are nearly equivalent (De Szoeke and Bennet 1993).

DOI: 10.1175/2009JPO4275.1

diapycnal mixing, the magnitude and spatial distribution of diapycnal mixing have a bearing on the abyssal circulation and stratification as well as on various aspects of the Meridional Overturning Circulation (MOC) (e.g., Munk and Wunsch 1998; Wunsch and Ferrari 2004). In turn, these have a bearing on the ability of the ocean to store and transport heat and greenhouse gases, and thus the parameterization of small-scale diapycnal mixing is a key ingredient to modeling large-scale ocean circulation as well as to the response of the climate system to natural and anthropogenic forcing (e.g; Saenko 2006; Kuhlbrodt et al. 2007).

Due to a lack of guiding observations and theories, diapycnal mixing has traditionally been parameterized as spatially uniform in OGCMs or varying only in the vertical (e.g., Bryan and Lewis 1979). However, relatively recent observations show that the spatial distribution of mixing is decidedly nonuniform. Weak mixing ($K_\rho \sim O(10^{-5}\ \mathrm{m^2\ s^{-1}})$) is expected over most of the deep ocean volume (e.g., Gregg 1987; Kunze and Sanford 1996) and enhanced, bottom-intensified mixing by several orders of magnitude is inferred over regions of rough topography (e.g., Gregg and Sanford 1980; Toole et al. 1997; Polzin et al. 1997; Finnigan et al. 2002; Klymak et al. 2006; Aucan et al. 2006; Kunze et al. 2006; Lozovatsky et al. 2008). The enhanced mixing is observed to persist even up to thousands of meters above the topography. A direct and nontrivial consequence of these observations is that mixing is depth dependent and patchily distributed horizontally.

Dynamically, vertical gradients of diapycnal mixing have a bearing on the intensity of upwelling via the buoyancy equation and the horizontal circulation via vorticity dynamics (e.g., McDougall 1991; St. Laurent 1999; St. Laurent et al. 2001; Saenko and Merryfield 2005; Katsman 2006). The observed spatial heterogeneity of turbulent mixing can thus be expected to have a profound impact on the ocean circulation. Early numerical studies of the sensitivity of the circulation to spatially localized mixing (e.g., Samelson 1998; Hasumi and Suginohara 1999) confirmed that global- and basin-scale circulation patterns calculated with localized mixing differ substantially from those obtained with spatially uniform mixing. A growing number of studies now demonstrate more specific consequences of nonuniform mixing on the ocean circulation. Some of the most important findings are that nonuniform mixing significantly alters the abyssal circulation from the classical Stommel–Arons pattern (e.g., Huang and Jin 2002; Katsman 2006), improves the representation of water masses (e.g., Simmons et al. 2004b; Koch-Larrouy et al. 2007), sets the deep ocean stratification (Saenko 2006), and results in a stronger and deeper Antarctic Circumpolar Current (e.g., Saenko and Merryfield 2005; Jayne 2009). Additionally, nonuniform mixing was found to affect the poleward heat transport (Simmons et al. 2004b), although later studies (Saenko and Merryfield 2005; Jayne 2009) indicate that the poleward heat transport is more affected by the value of diapycnal mixing in the upper ocean and thermocline than in the abyssal ocean. Clearly, the observed bottom-enhancement of mixing in regions of rough topography must be included in mixing parameterizations to improve our confidence in ocean circulation simulations.

In the past decade, a parameterization of mixing over rough topography due to the breaking of locally generated internal tides has been accomplished (e.g., St. Laurent 1999; Jayne and St. Laurent 2001; St. Laurent et al. 2002, hereafter JSL01). The JSL01 parameterization specifies the spatial distribution of mixing by the deterministic barotropic tidal currents and topographic roughness based on subcritical internal tide generation theory (Bell 1975). This work and subsequent implementation thereof in OGCMs (e.g., Simmons et al. 2004b; Saenko and Merryfield 2005) has conclusively shown that the general circulation cannot be considered decoupled from the tides (Jayne et al. 2004). In contrast, little progress has been made in parameterizing other components of topography-catalyzed mixing although these are likely to have a comparable impact on the spatial distribution of mixing. For instance, abyssal mixing can also be sustained by instability of internal lee waves associated with near-bottom mesoscale currents (e.g., Polzin and Firing 1997; Marshall and Naveira Garabato 2008), or by the interaction of remotely generated internal waves (e.g., near-inertial internal waves, low-mode internal tides radiating away from distant generation sites) with topography through reflection from a critical slope (e.g., Eriksen 1998; Legg 2003; Nash et al. 2004) or scattering off rough topography (Müller and Xu 1992). A recent numerical study (Saenko 2008) demonstrates that wind-driven abyssal flow can have magnitudes rivaling those of barotropic tidal flow over vast areas on seasonal time scales, thus potentially contributing significantly to abyssal mixing. Other processes contributing to topography-catalyzed mixing not yet parameterized include (but are not limited to) boundary layer turbulence (e.g., Armi 1978; Ivey 1987), hydraulic flow through constricted passages (e.g., Ferron et al. 1998; Thurnherr et al. 2005), and episodic overflow events at deep sills (e.g., Lukas et al. 2001). As is clear from this list, the tides are not the sole source of energy available for mixing the abyssal ocean; the wind is generally held to be a source of equal importance (e.g., Munk and Wunsch 1998; Wunsch and Ferrari 2004). Figure 1 is a rough sketch of energy flow from sources to dissipation near topography suggesting that tidalgenic mixing likely accounts

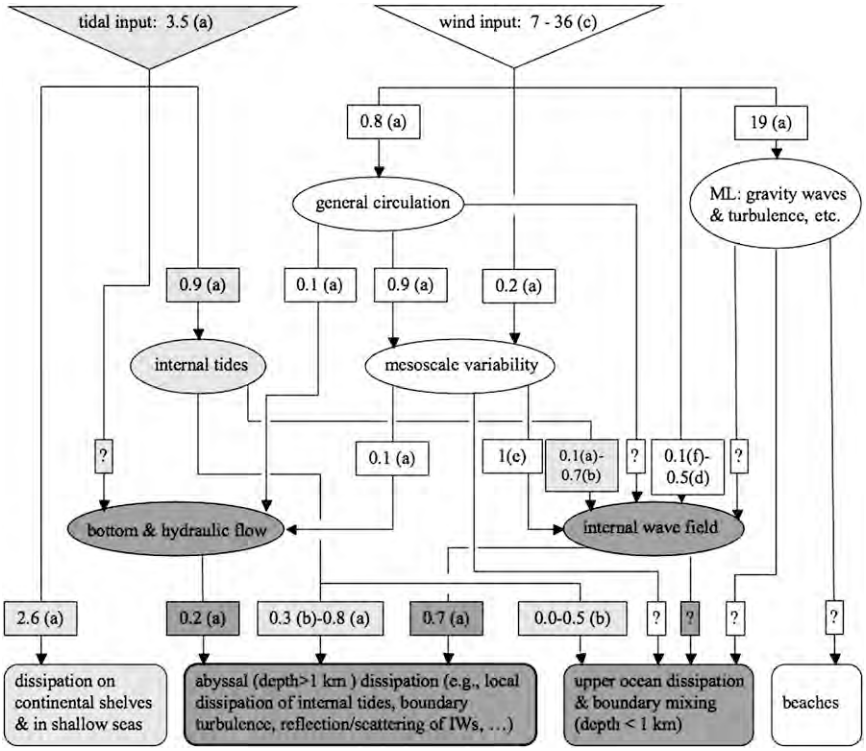

FIG. 1. Speculative energy paths from principal sources (top row) to dissipation [an update of Fig. 5 in Wunsch and Ferrari (2004)]. Fluxes are in TW with uncertainties of at least factors of 2 and possibly as large as 10. Shades are indicative of the dominant source of energy flux, with white corresponding to wind work, light gray to tidal work, and dark gray to a combination of both. Letters indicate references: (a) Wunsch and Ferrari (2004), (b) Jayne and St. Laurent (2001), (c) Lueck and Reid (1984), (d) Alford (2003), and (e) Williams et al. (2008). The astronomically determined tidal energy dissipation rate is 3.7 TW (Munk and Wunsch 1998), of which 0.2 TW drives the solid earth tides, leaving 3.5 TW to be dissipated in the ocean. It is believed that 2.6 TW are dissipated in the shallow seas and 0.9 TW is thought to be converted to internal tides. The wind stress causes inertial oscillations in the surface mixed layer with a flux of 0.5 TW into near-inertial internal waves. Surface gravity wave generation, Langmuir cells, and mixed layer turbulence by wind stress may take 19 TW, an unknown fraction of which goes into the internal wave field through resonant interaction and forcing at the base of the mixed layer. Roughly 1 TW of the wind work goes into the general circulation, which may leak energy to the internal wave field (e.g., through lee wave generation over rough topography) or directly produce near-bottom mixing though turbulence catalyzed by rough topography. Barotropic and baroclinic instabilities of the general circulation lead to mesoscale eddies, which in turn can lose energy to both the internal wave field through loss of balance roughly estimated to be $O(1)$ TW (Williams et al. 2008) and to mixing directly through bottom-catalyzed turbulence. Possible energy paths from eddies and mixing to the general circulation (see Wunsch and Ferrari 2004) and the $O(1)$ TW estimate of biomechanical work done by organisms swimming in the aphotic ocean (Dewar et al. 2006) are not shown.

for no more than half of the diapycnal mixing occurring in the abyssal ocean.

How one incorporates these processes and their important mixing effects into parameterizations remains a significant challenge. A complete description of topography-catalyzed mixing will likely be a function of the internal wave field, mesoscale currents, barotropic tidal velocities, plus the full three-dimensional structure of the topography. Major obstacles are the lack of resolution in both the OGCMs and global bathymetric datasets. Mesoscale eddies, let alone the internal wave field, are not adequately resolved in current OGCMs and neither are small-scale bathymetric features (horizontal scales less than 1 km), key to internal wave generation and scattering (e.g., Polzin 2004), in the best available global bathymetry [i.e., Smith and Sandwell (1997)

bathymetry; hereafter SS97]. Multibeam echosounder data do resolve small-scale topography but coverage of the ocean floor is still sparse.

We explore an empirical approach in this paper, assuming that the mean spatial distribution of diapycnal mixing depends primarily on height above bottom and a likely common denominator for topography-catalyzed mixing processes, topographic roughness. This approach is motivated by the observed dependence of bottom-enhanced mixing on topographic roughness (e.g., Kunze et al. 2006; Lozovatsky et al. 2008) and the observation that mean diapycnal diffusivity profiles inferred from microstructure data at different geographical locations tend to have a similar vertical decay structure, suggesting that a single functional form may adequately describe the vertical structure of diapycnal mixing resulting from a variety of physical processes and energy sources. In section 2b, a new metric for topographic roughness is introduced. The empirical model is described in section 2c. The vertical structure of K_ρ is assumed to decay as $K_b(r)[1 + h/h_0(r)]^{-2}$ with height above bottom h, based on the heuristic model for the decay of the turbulent kinetic energy (TKE) dissipation rate developed by Polzin (2004). The horizontal variability is introduced by assuming the maximum near-boundary diffusivity K_b and the scale height h_0 to be functions of topographic roughness r. Empirical fits for these two parameters as a function of topographic roughness are obtained from a collection of TKE dissipation rate profiles inferred from microstructure data. In section 3, this simple model for mean diapycnal mixing is shown to provide reasonable fits to the observations and to yield averaged diffusivities in rough agreement with bulk mixing rates inferred from large-scale hydrographic inversions, supporting the suggestion by Munk (1966) that boundary mixing followed by lateral transport of the mixed water into the ocean interior might be the mechanism sustaining the abyssal stratification. Moreover, given the simple model presented here, the power consumed by this mixing as it contributes to sustaining the observed stratification from the tropics up to midlatitudes is estimated to be less than 0.5 TW (TW = 10^{12} W) for the abyssal ocean, a requirement more comfortably reconciled with estimates of power injected into the abyssal ocean by tides and winds than the long-standing power consumption estimate of ~2 TW (Munk and Wunsch 1998).

2. Data and analysis

a. *Microstructure data: Evidence for topography-catalyzed mixing*

Microstructure profilers are highly specialized sensors capable of measuring the turbulent velocity shear on centimeter scales that can be directly related to the TKE dissipation rate ε. TKE dissipation rate profiles inferred from microstructure data from three different ocean regions are included in this analysis:

- Ninety-five profiles of the TKE dissipation rate were derived from High Resolution Profiler (HRP) microstructure data collected in 1991 around Fieberling Guyot, a seamount in the subtropical northeast Pacific Ocean (32°26′N, 127°46′W), as part of the Topographic Interactions Accelerated Research Initiative. (These profiles were generously provided by Dr. J. Toole.) For a detailed discussion of the HRP instrument and the calculation of ε, see Montgomery and Toole (1993). Analysis of the dataset is given in Toole et al. (1997), Kunze and Toole (1997), and Eriksen (1998). Nontidal internal wave reflection and diurnal tide–driven, vortex-trapped near-inertial internal waves atop of the seamount are thought to be responsible for most of the observed intensified mixing.
- A total of 165 full-depth profiles of the TKE dissipation rate were derived from HRP deployments acquired in 1996 and 1997 during the Brazil Basin Tracer Release Experiment (BBTRE), a component of the World Ocean Circulation Experiment. (These profiles were also provided by Dr. J. Toole.) The collective microstructure dataset spanned nearly 30° in longitude from the relatively smooth western Brazil Basin to the rough fracture zones of the Mid-Atlantic Ridge. The 1996 and 1997 datasets are henceforth referred to as Brazil Basin I and Brazil Basin II, respectively. A survey of the data is given in Montgomery (1998) and analysis is provided in St. Laurent (1999), Polzin et al. (1997), Zhang et al. (1999), Ledwell et al. (2000), St. Laurent et al. (2001), Morris et al. (2001), Polzin (2004), Thurnherr et al. (2005), and Toole (2007). The strong turbulence over the Mid-Atlantic Ridge has been attributed to internal waves generated by semidiurnal tidal flow over rough topography, shear due to near-inertial motions, and sill-related processes in ridge-flank canyons.
- Thirteen mean profiles of the TKE dissipation rate were derived from deployments of the deep Absolute Velocity Profiler (AVP) around the Hawaiian Islands ridge at French Frigate Shoals, Necker and Nihoa Islands, and the Kauai Channel. (These profiles were obtained courtesy of Drs. J. Klymak, T. Sanford, and J. Moum.) Each station was occupied for approximately 20 h, allowing four to six full-depth casts to be acquired and incorporated into the mean TKE profiles. For a detailed discussion of the calculation of ε with the AVP, see Lee et al. (2006). These data were collected as part of the 2000 Hawaiian Ocean

Mixing Experiment (HOME) field program described in Rudnick et al. (2003). Mixing around the Hawaiian ridge has been studied extensively (e.g., Finnigan et al. 2002; Merrifield and Holloway 2002; Klymak et al. 2006; Aucan et al. 2006; Carter et al. 2006; Lee et al. 2006; Levine and Boyd 2006; Martin et al. 2006; Rainville and Pinkel 2006a,b; Zaron and Egbert 2006; Klymak et al. 2008; Martin and Rudnick 2007; Aucan and Merrifield 2008). Intensified mixing near the Hawaiian Ridge has been attributed to local dissipation of the M_2 internal tide generated at the ridge, dissipation of near-inertial internal waves generated north of the ridge by winter storms, and strong nonlinear interactions via parametric subharmonic instability (PSI).

The AVP data were obtained preprocessed in the following way; TKE dissipation rates were computed spectrally over 5-m-depth intervals, which were then depth bin averaged into 100-m depth intervals $\langle\varepsilon\rangle$. Average diapycnal diffusivities $\langle K_\rho\rangle = \Gamma\langle\varepsilon\rangle/\overline{N^2}$ (Osborn 1980) were computed based on $\langle\varepsilon\rangle$, the survey mean stratification $\overline{N^2}$, and a mixing efficiency $\Gamma = 0.2$ (Oakey 1982). These estimates are considered conservative minima (Lee et al. 2006).

The TKE dissipation rate estimates collected by the HRP were obtained as 0.5-m binned averages. For the purposes of this work, these were further averaged over 10-m-depth bins. Integral time-scale estimates using the ARMAsel algorithm (Broersen 2002) indicated that an averaging length of 10 m is sufficient to obtain uncorrelated estimates of ε, consistent with the findings of Gregg et al. (1993). Diapycnal diffusivities K_ρ were obtained from the Osborn (1980) scaling using the 10-m depth bin-averaged TKE dissipation rates, a mixing efficiency of $\Gamma = 0.2$, and the local stratification profiles. The HRP profiles were obtained over a large geographical area and to varying depths. We therefore used the local stratification profiles since lateral variability in the background buoyancy frequency may incur serious errors when using a spatially mean stratification profile (e.g., Polzin 1992). For the HRP surveys used here, as well as for the AVP study around the Hawaiian Islands, the differences in the inferred K_ρ depending on whether the local profile or the survey mean stratification profile is used are minimal however. The stratification profiles were computed via the adiabatic leveling method (Bray and Fofonoff 1981) over 10-db pressure intervals centered about each dissipation estimate. TKE dissipation rates and diapycnal diffusivities were then bin averaged over 100-m height above bottom bins $\langle\varepsilon\rangle$ and $\langle K_\rho\rangle$. In the subsequent analysis, only data below 500 m of depth are considered to avoid enhanced dissipation from surface effects. Figure 2 shows the arithmetic[2] mean vertical profiles of the deep-ocean TKE dissipation rate $\langle\varepsilon\rangle$ and inferred diapycnal diffusivity $\langle K_\rho\rangle$ for the datasets discussed above. As a function of depth (not shown), no vertical structure is revealed. As a function of height above bottom, the mean diapycnal diffusivity profiles have maxima of $O(10^{-3})$ m^2 s^{-1} at the bottom boundary and decay with height above the bottom toward background values of $O(10^{-5})$ m^2 s^{-1}. The mixing is intensified at least up to 1 km from the bottom and thus the influence of topography-catalyzed mixing extends well into the stratified ocean interior. In contrast, the mean TKE dissipation rate profiles tend to have maxima near the bottom and near the surface due to the strong stratification in the upper ocean.

b. Topographic roughness

No global bathymetric dataset has the required resolution to adequately determine parameters such as the topographic slope, slope variance, curvature, and wavenumber content needed for a realistic prediction of topography-catalyzed turbulence and its decay above the seafloor. The SS97 global seafloor topography is currently the best available global topographic dataset, and although SS97 report data at 2 arc-minute resolution, the altimeter-derived topography does not accurately resolve features with spatial wavelengths less than about 2π times the ocean depth. We here nonetheless seek a simple and conservative measure of seafloor roughness based on SS97 bathymetry in the hope that some generic features of the topography-catalyzed turbulence may be captured. For this purpose, several seafloor roughness metrics based on SS97 and developed in the literature were examined, shown in Fig. 3 for the seamount-rich area north of the Enewetak and Bikini Atolls.

In the JSL01 tidal dissipation estimate (and in subsequent papers by these authors and coworkers), topographic roughness is characterized by (κ, h^2), the roughness wavenumber, and the amplitude scale. The amplitude scale h^2 is computed as the mean square residual height difference between the SS97 bathymetry and a polynomial sloping surface fit $Z = a + bx + cy + dxy$ over $0.5° \times 0.5°$, nonoverlapping cells. (The choice of $0.5° \times 0.5°$ cells was motivated by the grid size of the tidal model used.) The wavenumber κ is not estimated from the topography but treated as a free parameter tuned to minimize the difference between the modeled

[2] The mean vertical diffusivity profile was also computed using the maximum likelihood estimator described in Baker and Gibson (1987). We found that the microstructure data are sufficiently densely sampled to allow the use of the arithmetic mean without significant bias.

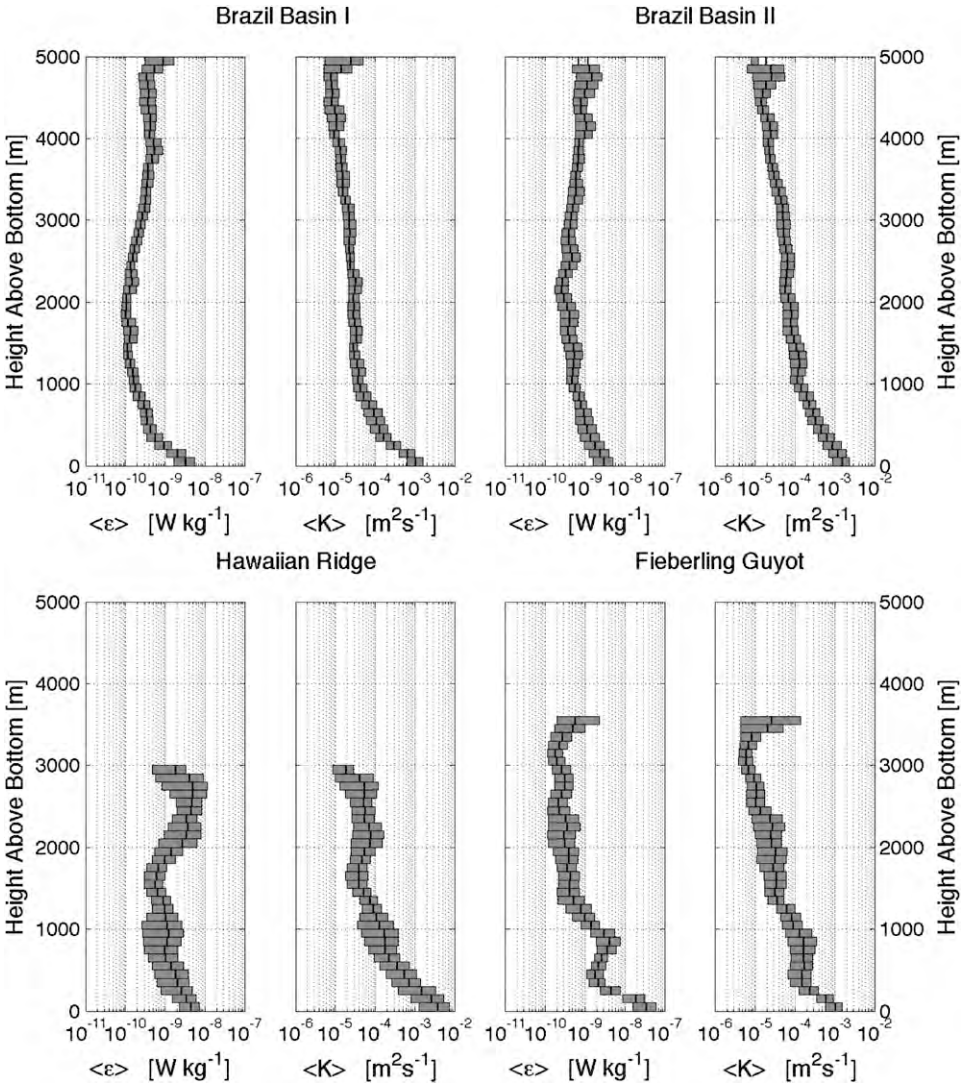

FIG. 2. Mean vertical profiles of TKE dissipation rates $\langle \varepsilon \rangle$ and diapycnal diffusivities $\langle K_\rho \rangle$ for each microstructure dataset smoothed over 500 m. Both $\langle \varepsilon \rangle$ and $\langle K_\rho \rangle$ are bin averaged over 100-m height above bottom intervals. Only data from depths >500 m are employed. The gray bins denote 95% bootstrap confidence intervals.

and observed barotropic tides. In Fig. 3, the quantity κh^2 is plotted with $\kappa = 2\pi/10$ km. Gille et al. (2000) computed roughness on a 0.25° latitude × 0.2° longitude grid by first applying a high-pass filter (retaining wavelengths $\lambda < 160$ km) to SS97 bathymetry, squaring the filtered bathymetry, applying a low-pass filter (retaining wavelengths $\lambda > 160$ km) and then taking the square root. Kunze et al. (2006) defined the topographic roughness as the variance of the SS97 bathymetry in 32 km × 32 km boxes. In the present study, we opt for a root-mean-square approach in the vein of Gille et al. (2000) but at the resolution of the SS97 bathymetry since we are not tied to the grid size of a numerical model. We define the seafloor roughness r as the weighted RMS height of the SS97 bathymetry H (which is already a smoothed version of the true bathymetry); that is,

$$r = \langle (H - \langle H \rangle)^2 \rangle^{1/2}. \tag{1}$$

The weighted mean of the bathymetry H is here given by $\langle H \rangle = \sum_i w_i H_i$, where the sum is carried out over all grid points contained within a circle of radius l. The weighting function is a Gaussian $w_i(s) = A \exp(-s_i^2/2\sigma^2)$ with standard deviation $\sigma = l/2$, s the radial distance from the center of the circle, and normalization constant $A = 1/\sum_i w_i$. The weighting function was introduced to limit

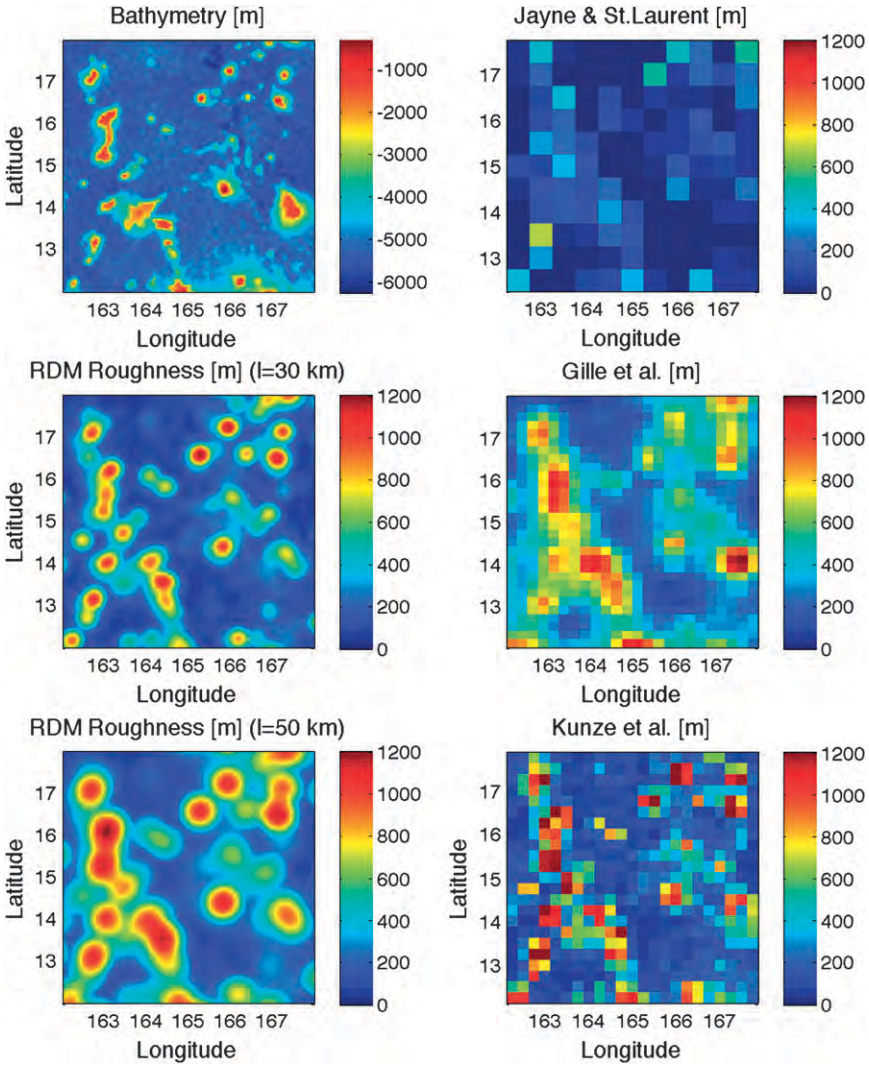

FIG. 3. Roughness metrics of a seamount-rich area in the western Pacific: (top left) bathymetry and RDM roughness with l = (middle left) 30 and (bottom left) 50 km. Four different methods of quantifying the roughness are compared here: Eq. (1) vs methods by (middle right) Gille et al. (2000), (top right) Jayne and St. Laurent (2001) (κh^2 shown), and (bottom right) Kunze et al. (2006). Results from Eq. (1) are shown for two different values of l, the radius of the circular area used to calculate the mean. Equation (1) with = 30 km, considered more conservative, is used in this study because large roughness values associated with steep seamounts are not spread over large areas. Units for roughness are m.

the horizontal smearing of large roughness values calculated at sharp topographic features. The effect of varying the circle of influence of the weighting function is shown in Fig. 3. While Eq. (1) is a subjective measure of seafloor roughness, it is also conservative in the sense that the influence of sharp topographic features remains localized and it appears to be more reflective of the underlying bathymetry than other schemes (Fig. 3). A value of l = 30 km was judged to be appropriate, because (i) acute topographic features are not spread over large areas with this value and (ii) reducing l further results in the increasing importance in r of short-scale structures dependent on short-scale bottom slopes that are not reliable in the bathymetric dataset that is already a spatially smoothed representation of the seafloor topography. A more in-depth investigation of the impacts of the choice of seafloor roughness metric on the diffusivity model presented here will be the subject of a future investigation. A global map of the topographic roughness r and its distribution are shown later (top panels of Fig. 7). The roughness r reaches values as high as 1000 m but 95% of the seafloor has values between 0 and 400 m.

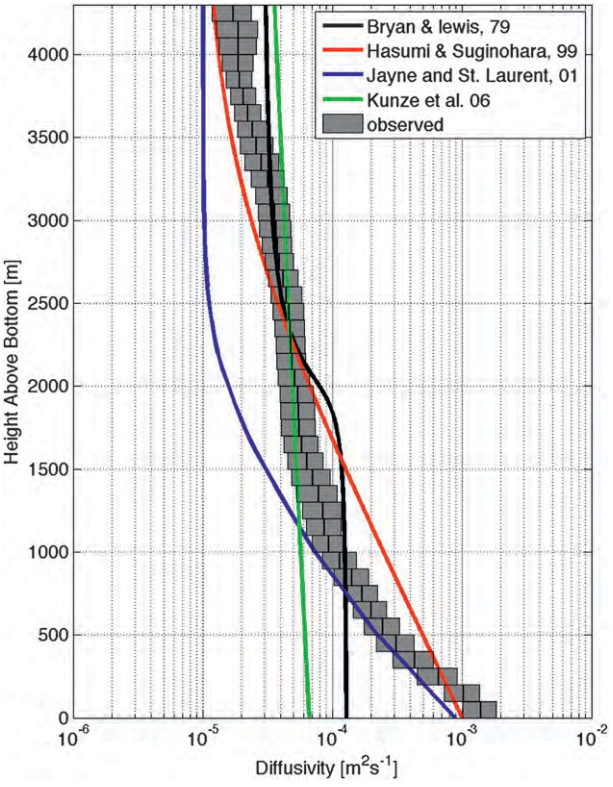

FIG. 4. Comparison of various proposed vertical structure functions to the mean diapycnal diffusivity profile inferred from the observed TKE dissipation rates. Gray bins indicate 95% bootstrap confidence intervals for 100-m height above bottom bins. The Bryan and Lewis (1979) profile is independent of position. Hasumi and Suginohara (1999) used the profile shown for areas considered to be rough and the Bryan and Lewis profile for smooth areas. The Jayne and St. Laurent (2001) and Kunze et al. (2006) profiles have a maximum boundary value varying geographically depending on the expected magnitude of the barotropic tide and topographic roughness but use constant decay-scale heights of 500 and 5500 m, respectively, independent of location.

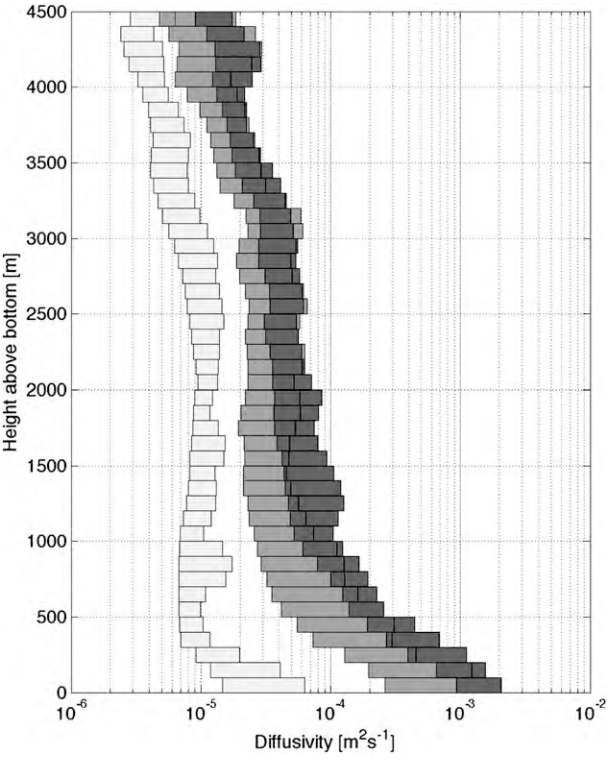

FIG. 5. The 95% bootstrap confidence intervals of the mean diffusivity profiles based on data from locations with roughness values between 0 and 100 m (smooth), 50 and 150 m (intermediate), and 100 and 300 m (rough) to illustrate the changing mean vertical profile of K_ρ as topographic roughness increases.

c. *A simple model for $K_\rho(x, y, z)$*

While horizontally localized mixing is now recognized to be significant to the global abyssal mixing problem, the vertical structure of turbulent mixing has been somewhat neglected. Hasumi and Suginohara (1999) noted that the difference in the deep-ocean circulation between two of their model runs was the consequence of a different vertical profile of diapycnal diffusivity rather than horizontal inhomogeneity, indicative that realistic distributions of diffusivity in both the horizontal and vertical are important to simulating the MOC. Typical proposed vertical structure functions are exponential or simpler, and independent of location. For instance, global extrapolations of observed or predicted locally enhanced mixing are often based on the area fraction approach introduced by Armi (1978), which is equivalent to a step function for the vertical profile of diffusivity (e.g., Garrett and Gilbert 1988; Toole et al. 1997). OGCMs often employ the ad hoc arctangent profile introduced by Bryan and Lewis (1979). The vertical structure function of the TKE dissipation rate employed in the JSL01 tidal dissipation parameterization is an exponential profile with a decay scale of 500 m at all locations [which is converted to a vertical profile of diffusivity using Osborn's (1980) relation]. This choice is roughly consistent with observations, though described as somewhat arbitrary by St. Laurent and Nash (2003). Kunze et al. (2006) fit an exponential profile to about 3500 diapycnal diffusivity profiles based on the Gregg et al. (2003) finescale parameterization applied to lowered acoustic Doppler current profiler (LADCP)–CTD profiles from the World Ocean Circulation Experiment. They found a decay scale of 5500 $\pm$ 1500 m for bottom diffusivities greater than 0.5×10^{-4} m^2 s^{-1} and decay scales much larger than the ocean depth for smaller bottom diffusivities. Figure 4 compares the above-mentioned vertical profiles (except for the step function) to the mean vertical profile of diffusivity derived from the microstructure data considered here and illustrates that each only

crudely captures the mean vertical structure of the observations; in particular, none capture the curvature in the bottom 2 km. Figure 5 shows mean observed diffusivity profiles for different topographic roughness ranges and summarizes the structure the empirical model developed here aims to parameterize as a function of height above bottom and topographic roughness:

- the mean diffusivity decreases with height above bottom (unlike the TKE dissipation rate, which tends to have both near-bottom and near-surface maxima due to the strong stratification in the upper ocean),
- the maximum diffusivity near the boundary increases with seafloor roughness, and
- the mean vertical profiles show curvature in lognormal space.

No obvious latitudinal variation of diapycnal diffusivity, as reported by Gregg et al. (2003) and Hibiya et al. (2006) could be inferred from the data, perhaps due to the limited number of latitudes sampled. Insofar as the microstructure data have been taken from regions of the ocean with quite different relative contributions of tidal, internal wave, mesoscale, etc., energy sources for diapycnal mixing, the successful discrimination of distinct diffusivity profiles based on just a topographic roughness metric is an encouraging result for the prospect of producing a refined parameterization of deep-ocean mixing that will not be prohibitively sensitive to the mix of processes creating the turbulence.

Polzin (1999, 2004, 2009) developed a heuristic recipe for assessing the vertical decay of bottom-generated internal waves and obtained idealized expressions for the vertical profile of the TKE dissipation rate and diffusivity that do capture the observed decay with height above bottom reasonably well (see Figs. 4 and 5 in Polzin 2004). Polzin (2004) interpreted observations of bottom-enhanced diapycnal mixing in the Brazil Basin as the signature of an enhanced internal wave field due to a combination of internal wave generation and scattering off topographic features with small horizontal scales (<1 km). The turbulent dissipation is assumed to be the end result of the downscale transport of energy associated with nonlinear wave–wave interactions as the bottom-generated internal waves propagate upward [see also Mackinnon and Winters (2003) for profiles of the TKE dissipation rate obtained from bottom-generated internal waves]. Based on semiempirical flux laws representing the nonlinear transfer of energy due to wave–wave interactions, the vertical profile of the TKE dissipation rate was found to decay with distance from the bottom as $\varepsilon = \varepsilon_0/(1 + h/h_0)^2$, where h is the height above the bottom, ε_0 a maximum boundary dissipation rate, and h_0 a decay scale height. The parameters ε_0, h_0 are functions of the unresolved internal wave field at the bottom boundary and would need to be determined from models of wave generation and scattering. We here seek to parameterize the diapycnal mixing in terms of resolved parameters, however, and simplify the problem by adopting a vertical dependence for diapycnal diffusivity identical to Polzin's theoretical vertical structure for the TKE dissipation rate (this would follow, for instance, if one applied the Osborn relation mentioned earlier with constant buoyancy frequency and mixing efficiency, not unreasonable low-order approximations in the abyssal ocean). Consequently, the form of the diffusivity as a function of height above the bottom, h, is assumed to be

$$K_\rho(h, r) = K_b(r)[1 + h/h_0(r)]^{-2} + K_{\text{back}}, \qquad (2)$$

where the maximum boundary diffusivity $K_b(r)$ and scale height $h_0(r)$ are functions of the topographic roughness only and $K_{\text{back}} = 5.6 \times 10^{-6}$ m^2 s^{-1} is the background diffusivity associated with background Garret–Munk internal wave conditions assuming a mixing efficiency of $\Gamma = 0.2$ (Polzin et al. 1995). This choice of K_{back} accommodates the many observations that are inferior to the traditional background diffusivity of 10^{-5} m^2 s^{-1}. Henceforth, we will refer to Eq. (2) as the roughness diffusivity model (RDM). Conceptually, the RDM is akin to assuming that the ocean is replete with background currents of tidal and lower frequencies, and that there are numerous processes modifying these currents and the ambient internal wave field itself near rough topography, leading to an energized internal wave field and enhanced mixing. How much the mixing is enhanced is assumed to depend only on the details of the topography and will be addressed empirically. The choice to cast the RDM in terms of diffusivity rather than the TKE dissipation rate is based on the Henyey et al. (1986) wave–wave interaction model. Polzin et al. (1995) examined several wave–wave interaction models against micro- and fine structure data and found the most support for the Henyey et al. (1986) model, implying that $\varepsilon \propto N^2$, and thus that the diapycnal diffusivity is independent of the stratification (Toole 1998). A parameterization for diapycnal diffusivity can therefore be applied globally in spite of the spatial variability of the stratification. Next, we seek functions describing $K_b(r)$ and $h_0(r)$ empirically from the $\langle K_\rho \rangle$ profiles inferred from the observed TKE dissipation rate profiles.

The parameters K_b and h_0 are estimated for each of the 273 $\langle K_\rho \rangle$ profiles separately [i.e., with topographic roughness appropriate to each profile, according to Eq. (1) with $l = 30$ km] through nonlinear regression using the Gauss–Newton algorithm with Levenberg–Marquardt modifications for global convergence (Seber and Wild

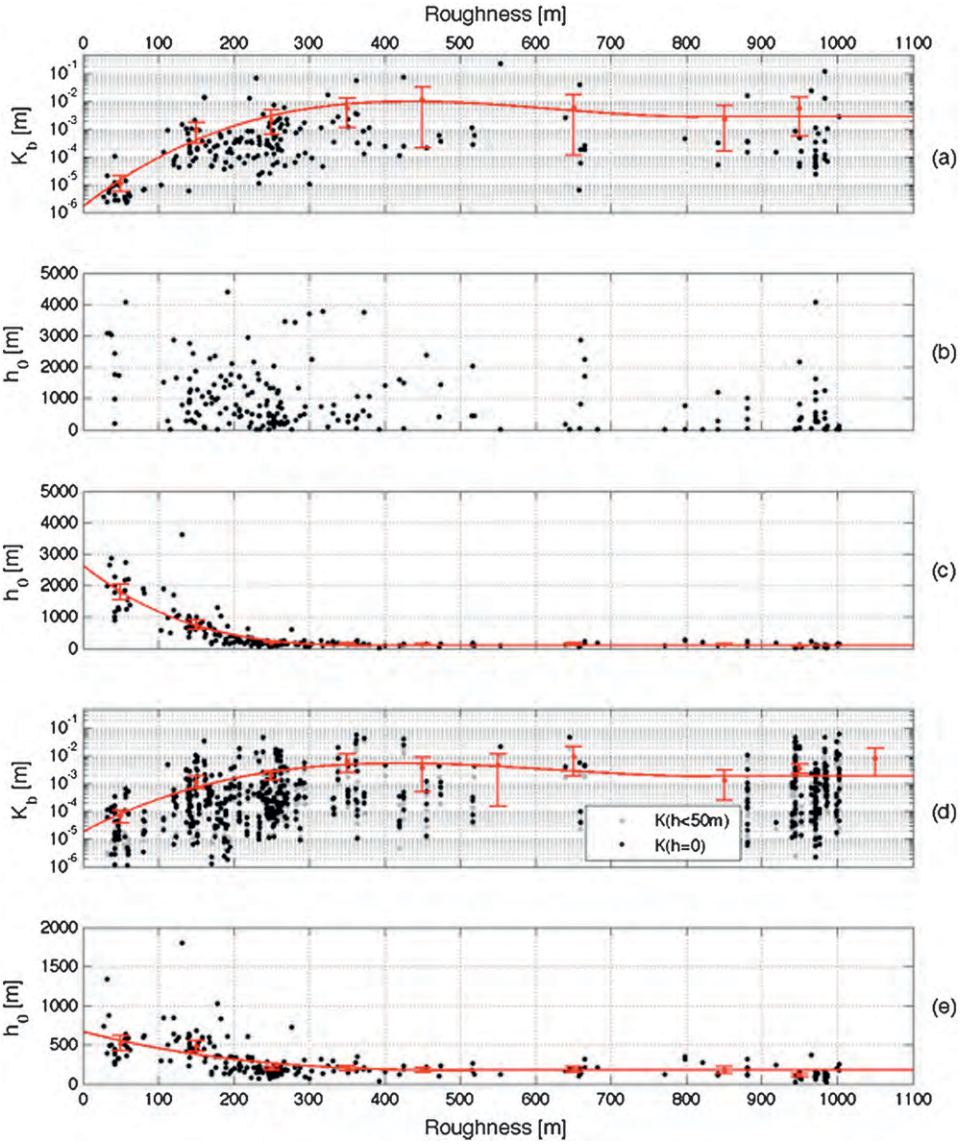

FIG. 6. (a),(b) The boundary diffusivity $K_b(r)$, and scale heights $h_0(r)$ (black dots) when determined simultaneously through nonlinear regression on the $\langle K_\rho \rangle$ profiles. In (a), red shows mean $K_b(r)$ binned in 100-m roughness intervals with 95% bootstrap confidence intervals. The red line is a third-order polynomial fit in log space to the mean $K_b(r)$. (c) Black dots show $h_0(r)$ determined from nonlinear regression on the $\langle K_\rho \rangle$ profiles with $K_b(r)$ fixed to the polynomial fit shown in (a). Red shows mean $h_0(r)$ binned in 100-m roughness intervals with 95% bootstrap confidence intervals. The red line is a third-order polynomial fit to the mean $h_0(r)$. (d) Near-boundary diffusivities $K_\rho(h < 50$ m) inferred from the microstructure data (gray dots) and their projected values at the boundary $K_\rho(h = 0)$ (black dots) using Eq. (2) with scale heights specified by the polynomial in (c). Red shows the means of the projected $K_b(r)$ binned in 100-m roughness intervals with 95% bootstrap confidence intervals. The red line is a third-order polynomial fit in log space to the mean $K_b(r)$. (e) Black dots show $h_0(r)$ determined from nonlinear regression on the $\langle K_\rho \rangle$ profiles with $K_b(r)$ fixed to the polynomial fit shown in (d). Red shows mean $h_0(r)$ binned in 100-m roughness intervals with 95% bootstrap confidence intervals. The red line is a third-order polynomial fit to the mean $h_0(r)$. The polynomial fits for $K_b(r)$ and $h_0(r)$ shown in (d) and (e) are used for the roughness diffusivity model.

1989). Figures 6a and 6b, respectively, show $K_b(r)$ and $h_0(r)$ when both are treated as free parameters in the nonlinear regression. There is considerable scatter, yet both plots exhibit some structure. The boundary diffusivities inferred from the regression increase from a range of $O(10^{-6}$–$10^{-4})$ to a range of $O(10^{-4}$–$10^{-1})$ $m^2\ s^{-1}$ as the topographic roughness increases from 0 to 400 m and then decrease slightly for higher roughness values. The decay scale heights inferred from the regression range from $O(10$ m) to $O(1000$ m) with most of the large decay scales occurring at topographic roughness values below 400 m. A least squares third-order polynomial fit to the inferred K_b binned in 100-m roughness intervals is shown in red in Fig. 6a. Repeating the nonlinear regression with this simple functional form for $K_b(r)$ yields a clear pattern in the scale heights as a function of topographic roughness (see Fig. 6c). The scale heights decrease rapidly from roughly 2500 to 100 m as the topographic roughness increases to 400 m and then remain constant for higher roughness values. A least squares third-order polynomial fit to the inferred h_0 binned in 100-m roughness intervals is shown as the red line in Fig. 6c.

A more conservative estimate for $K_b(r)$ was subsequently constructed based on observed diffusivities within 50 m from the bottom. Given the scale height parameterized as the polynomial function discussed above, $K_b(r)$ was estimated from observed diapycnal diffusivities within 50 m from the bottom as $K_\rho(h = 0)$ using Eq. (2). These were binned in 100-m roughness intervals and parameterized as a least squares third-order polynomial fit (red line in Fig. 6d):

$$K_b(r) = \begin{cases} K_{\mathrm{bo}} \exp[k_1(r/r_0)^3 + k_2(r/r_0)^2 + k_3(r/r_0)]; & r \le 830 \\ 1.8 \times 10^{-3}; & r > 830 \end{cases}, \tag{3}$$

where $k_1 = 3 \times 10^{-8}$, $k_2 = -5.8 \times 10^{-5}$, $k_3 = 0.0325$, and $K_{\mathrm{b0}} = \exp(k_4) = 1.87 \times 10^{-5}$ $m^2\ s^{-1}$. The constant boundary diffusivity for topographic roughness values larger than 830 m was introduced to avoid changes in $K_b(r)$ at large roughness values unconstrained by the data. Since no typical roughness value is determined on either an observational or theoretical basis, the normalization constant r_0 was assigned a value of 1 m for dimensional consistency. Using $K_b(r)$ specified by (3), the nonlinear regression was repeated to determine a new $h_0(r)$. The scale heights obtained from the regression with $K_b(r)$ given by (3) decrease from a maximum at 670 m to 170 m at a roughness value of 540 m, after which they remain level. A least squares third-order polynomial fit to the 100-m roughness binned scale heights yields (Fig. 6e)

$$h_0(r) = \begin{cases} a_1(r/r_0)^3 + a_2(r/r_0)^2 + a_3(r/r_0) + a_4; & r \le 540 \\ 170; & r > 540 \end{cases}, \tag{4}$$

where $a_1 = -2.9 \times 10^{-6}$, $a_2 = 0.0046$, $a_3 = -2.5896$, and $a_4 = 670$ m. A constant scale height for roughness values greater than 540 m was introduced to avoid unphysical behavior at larger roughness values. Further repetition of this procedure, that is, estimating a new $K_b(r)$ based on observed diffusivities within 50 m of the bottom via Eq. (2) with $h_0(r)$ given by (3), yielded no significant changes to either $K_b(r)$ or $h_0(r)$; they will be specified by Eqs. (3) and (4) for the remainder of the paper.

A global map of the boundary diffusivity $K_b(r)$ obtained from Eq. (3) is shown in Fig. 7 (bottom). The magnitude and spatial variation have similarities to predictions of boundary diffusivity based on the JSL01 parameterization (e.g., Fig. 1 of St. Laurent et al. (2002)) but notable differences exist, in particular in the Southern Hemisphere over the mid–Indian Ridge, the southeast Indian Ridge, sections of the East Pacific Rise, the Chile Rise, and the Pacific–Antarctic Ridge, all regions of relatively weak barotropic tidal dissipation (Egbert and Ray 2001; Egbert and Ray 2003).

The joint variation of the maximum boundary diffusivity and scale height with topographic roughness leads to simple vertical profiles of diapycnal diffusivity as shown in Fig. 8 for several roughness values. Over smooth topography, the diffusivities are low near the bottom and decay slowly (scale heights $\ge$500 m) toward background values, whereas the enhanced diffusivities over rough topography are associated with fast decay (small scale heights $\sim$150 m). The inclusion of a background diffusivity has no effect on the scale heights inferred from nonlinear regression for roughness values greater than 100 m. For lower roughness values, scale heights inferred without a background diffusivity are larger by several hundred meters to prevent diffusivities from decaying below observed values several 1000 m from the bottom. The use of a background diffusivity reduces the excessively large scale heights and allows for a better fit of the near-bottom decay of diffusivity at low roughness values. Note that for small roughness values, our choice of background diffusivity

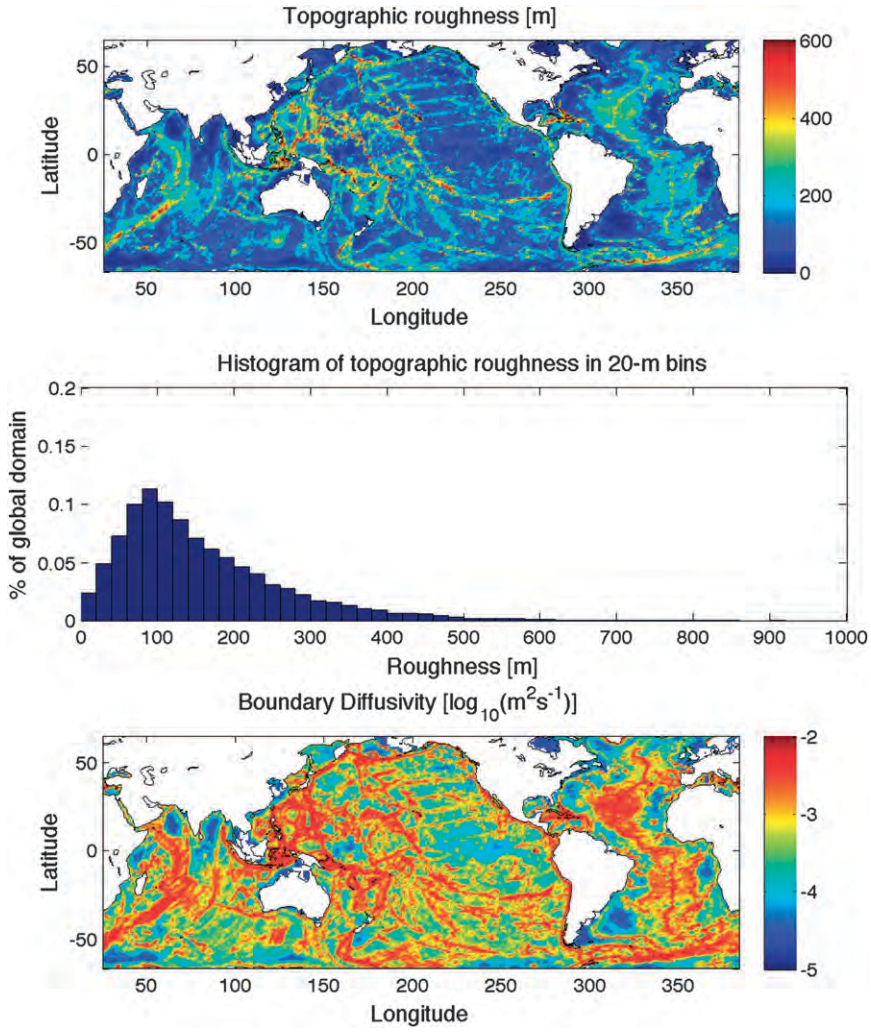

FIG. 7. (top) A global map of topographic roughness in 1° × 1° averages obtained from Eq. (1). (middle) The distribution of topographic roughness, where 95% of the global seafloor has roughness values between 0 and 400 m. (bottom) A global map of the boundary diffusivities obtained from the RDM [Eq. (3)]. The magnitudes and spatial distribution are comparable to the boundary diffusivities predicted by the JSL01 parameterization. Higher boundary diffusivities are predicted by the RDM over the mid–Indian and southeast Indian Ridges, sections of the East Pacific Rise, the Chile Rise, and the Pacific–Antarctic Ridge (cf. Fig. 1 in St. Laurent et al. 2002).

($K_{back} = 5.6 \times 10^{-6}$ m^2 s^{-1}) allows the modeled diffusivity to be less than 10^{-5} m^2 s^{-1}, considered by many authors (e.g., Munk and Wunsch 1998; St. Laurent et al. 2002) to be a reasonable background diffusivity in the open ocean. In fact, the diffusivities estimated from the microstructure data, as well as the many diffusivities estimated by Kunze et al. (2006), frequently have values smaller than 10^{-5} m^2 s^{-1} away from rough topography.

Figure 9 compares the mean of the diapycnal diffusivity profiles predicted by the RDM at the locations of all microstructure profiles to the observed mean vertical profile for each microstructure survey considered here. These mean predicted profiles differ from the observed mean profiles by no more than a factor of 2 for each survey. The predicted profile for all the data shows that the simple model captures the mean structure of the observed diffusivity to within 95% confidence intervals in the first 1500 m above the bottom and may be on the conservative side (i.e., weaker than observed) higher up in the water column. Note that an exponential decay with a fixed decay scale of 500 m as in the JSL01 parameterization (see the blue profile in Fig. 4) underestimates the mean observed diffusivity from 1000 m above the bottom upward and differs by factors of 5

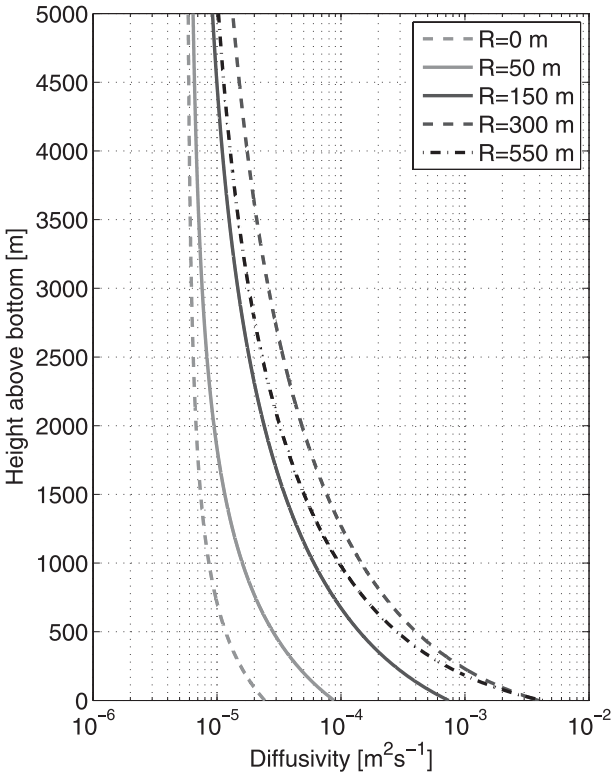

FIG. 8. Vertical profiles of diapycnal diffusivity obtained from the RDM for various roughness values. Note that the profile with $r = 550$ m has a smaller scale height than the profile for $r = 300$ m and thus decays faster.

between 2000 and 3000 m from the bottom. Predictions from the RDM agree with the mean of all the data to within a factor of 2 at all heights above the bottom. For simplicity, a factor of 2 will be used to indicate a plausible uncertainty range for the predicted mean diffusivity profiles.

The bottom-right panel of Fig. 9 compares the mean of the diapycnal diffusivity profiles predicted by the RDM to the observations for topographic roughness intervals ranging from smooth to rough. The predicted profile for the smooth range (0–100 m) overestimates the observations in the first 1200 m above bottom but remains within a factor of 2. For the intermediate (50–150 m) and rough (100–300 m) ranges, the predictions are within the 95% confidence intervals for the first 1500 m above the bottom and are on the conservative side (i.e., smaller) higher up in the water column. The fits for heights greater than 1500 m above bottom may be improved by allowing the scale height to increase as a function of height above bottom, as suggested by the analysis in Polzin (2004). The dependence of the scale height on height above bottom could not be inferred from the data analyzed here but this is an avenue for further refinement. Overall, the comparison illustrates that the variation of boundary diffusivity with topographic roughness is captured by the RDM and that the decrease of scale height with topographic roughness forms an improvement over a fixed decay scale at all locations, which would simply result in the same vertical profile for all roughness values but shifted along the abscissa with varying topographic roughness.

3. Discussion and results

Three-dimensional maps of the turbulent diapycnal diffusivity can now be constructed based on the RDM [Eqs. (2)–(4)] and the topographic roughness derived from SS97 bathymetry [Eq. (1) with $l = 30$ km]. Given the stratification, the diffusivities can be converted to TKE dissipation rates using the Osborn (1980) relation $\varepsilon = K_\rho N^2/\Gamma$ with $\Gamma = 0.2$, as before. The buoyancy frequency profiles used here to obtain ε are $1° \times 1°$ averages derived from the 2005 *World Ocean Atlas* (*WOA*) temperature and salinity profiles. Figure 10 displays resulting global maps of K_ρ and ε at depths of 1 and 3 km. Whether any specific high-roughness region actually exhibits the levels of mixing and dissipation implied by Fig. 10 will of course depend on the nature of the available energy sources such as the tides, wind-generated internal waves, and low-frequency mesoscale variability, whose individual energy levels vary significantly as a function of location. Our RDM and resultant dissipation rates are primarily intended to provide a more systematic extrapolation of the sparse observed diffusivities than has been accomplished previously. They are not intended to provide definitive maps of the spatial dependencies of K_ρ and ε in the deep ocean.

However, insofar as the microstructure data upon which the RDM is based have been taken from regions of the ocean with quite different relative contributions of tidal, internal wave, mesoscale, etc., energy sources for diapycnal mixing, the successful discrimination of distinct diffusivity profiles based on just a topographic roughness metric suggests that the sum total of all energy sources contributing to topography-catalyzed mixing may have a more uniform horizontal dependence than any of the individual energy contributors. As for the boundary diffusivity map shown in Fig. 7, the maps in Fig. 10 do exhibit many similarities with published maps of predicted intensified mixing due to local dissipation at internal tide generation sites (e.g., St. Laurent et al. 2002; Simmons et al. 2004a), while the differences provide suggestions for locations where future explorations of nontidal mixing phenomena might be profitably focused. An interesting difference between Fig. 10 and published maps of tidalgenic mixing based on the JSL01

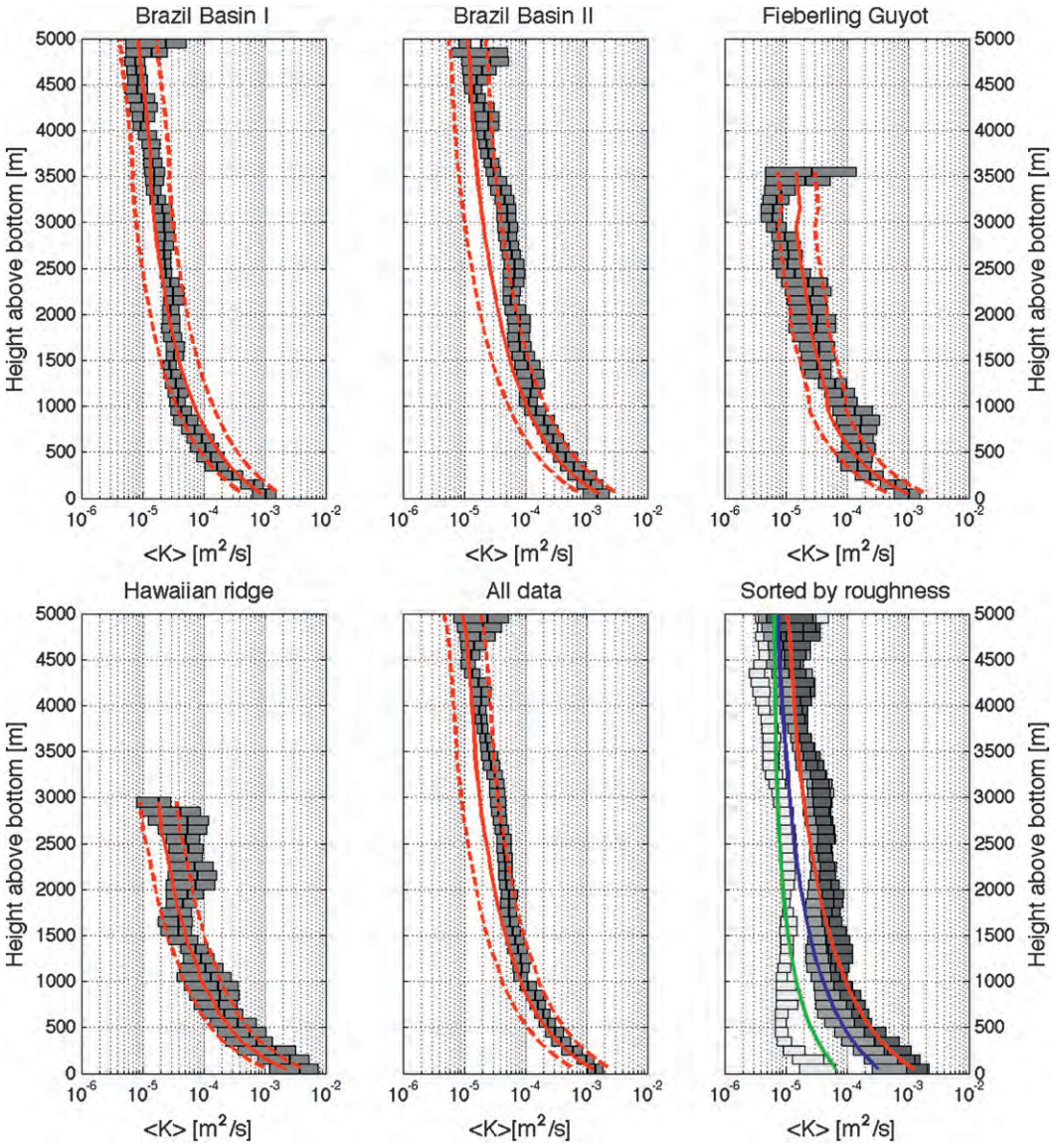

FIG. 9. Mean diapycnal diffusivity profiles (red) predicted from the RDM and factors of 2 thereof (dashed red) compared to mean profiles for each microstructure dataset with 95% bootstrap confidence intervals in gray. The bottom-right panel shows 95% bootstrap confidence intervals of mean diffusivity profiles for different roughness ranges as in Fig. 5 and mean predictions from the RDM for the smooth range (green), intermediate range (blue), and rough range (red).

parameterization arises from the difference in the vertical structure functions. A distinct horizontal structure remains apparent in the RDM predictions at 1 km of depth, whereas diffusivities predicted by the JSL01 parameterizations at 1 km have decayed toward background values at nearly all locations (cf. Fig. 1 of St. Laurent et al. 2002). Note that both the vertical structure function of the RDM and the JSL01 parameterization result are biased low compared to the mean observed profile upward of 1500 m from the bottom but the RDM remains within a factor of 2 from the observations whereas the exponential decay employed in the JSL01 parameterization differs by up to a factor of 5. The numerical studies by Saenko and Merryfield (2005) and Jayne (2009) suggest that the diapycnal diffusivity at this depth and upward have a bearing on the poleward heat transport. Furthermore, given the approximate area of the low-latitude ocean at that depth ($\sim 2.35 \times 10^{14}$ m^2 between 40°S and 48°N based on SS97 bathymetry), the average predicted diffusivity of $K_\rho = 3 \times 10^{-5}$ m^2 s^{-1} by the RDM can account for about 7 Sv (1 Sv $\equiv 10^6$ m^3 s^{-1}) [$A \times w \approx K_\rho \times (A/h)$, with $h = 1$ km] of dense-to-light

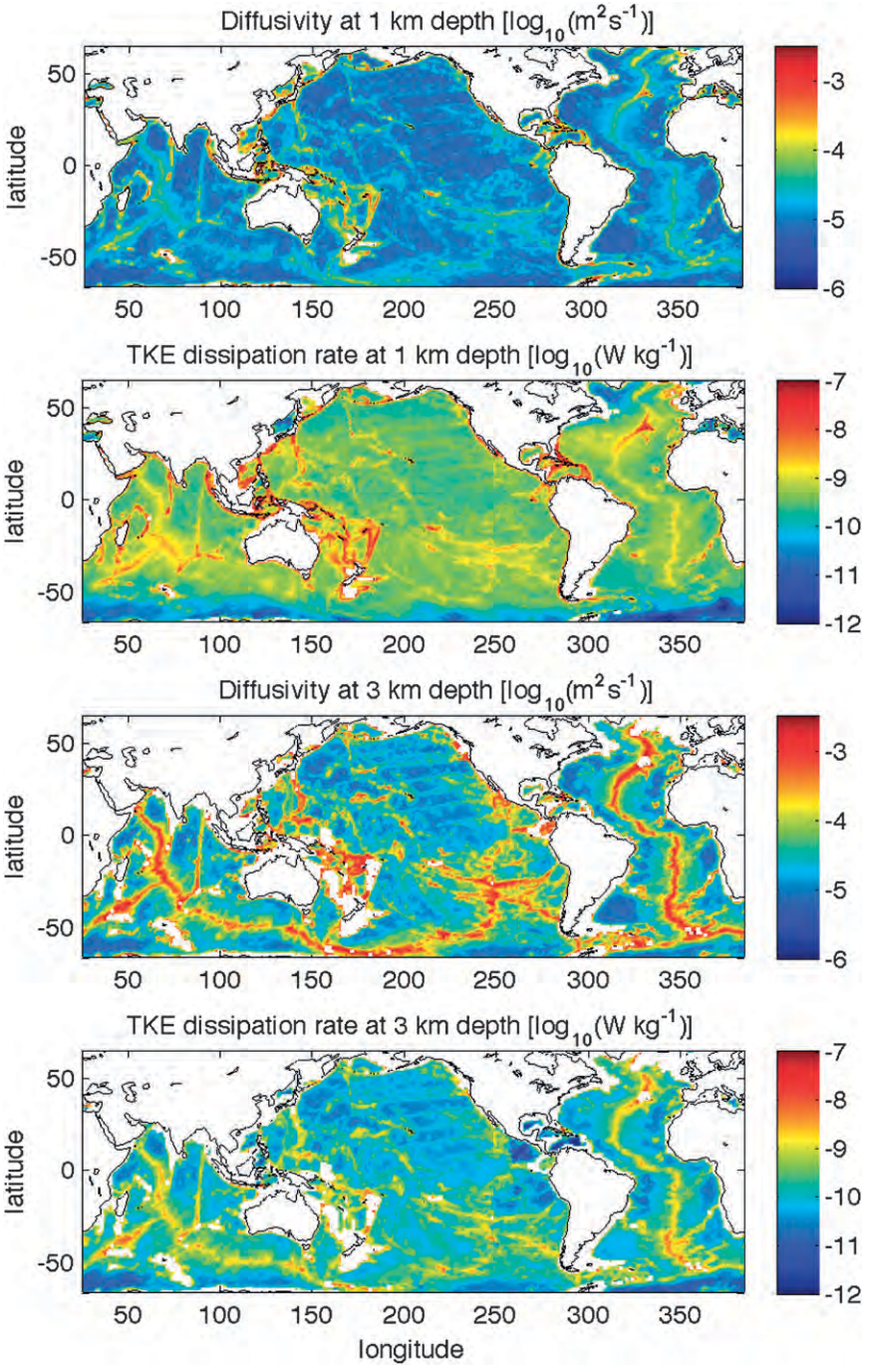

FIG. 10. Global diapycnal diffusivity at (top) 1- and (third panel) 3-km depth and TKE dissipation rate obtained from the RDM at depths of (second panel) 1 and (bottom) 3 km. Note that the spatial variations of the TKE dissipation rates at 1-km depth are not only dependent on the topographic roughness, but also on the lateral variability of the stratification. At the 3-km-depth level, the TKE dissipation rates vary mainly as a function of topographic roughness. Values shown here are $1° \times 1°$ averages; blank areas are shallower than the given depth.

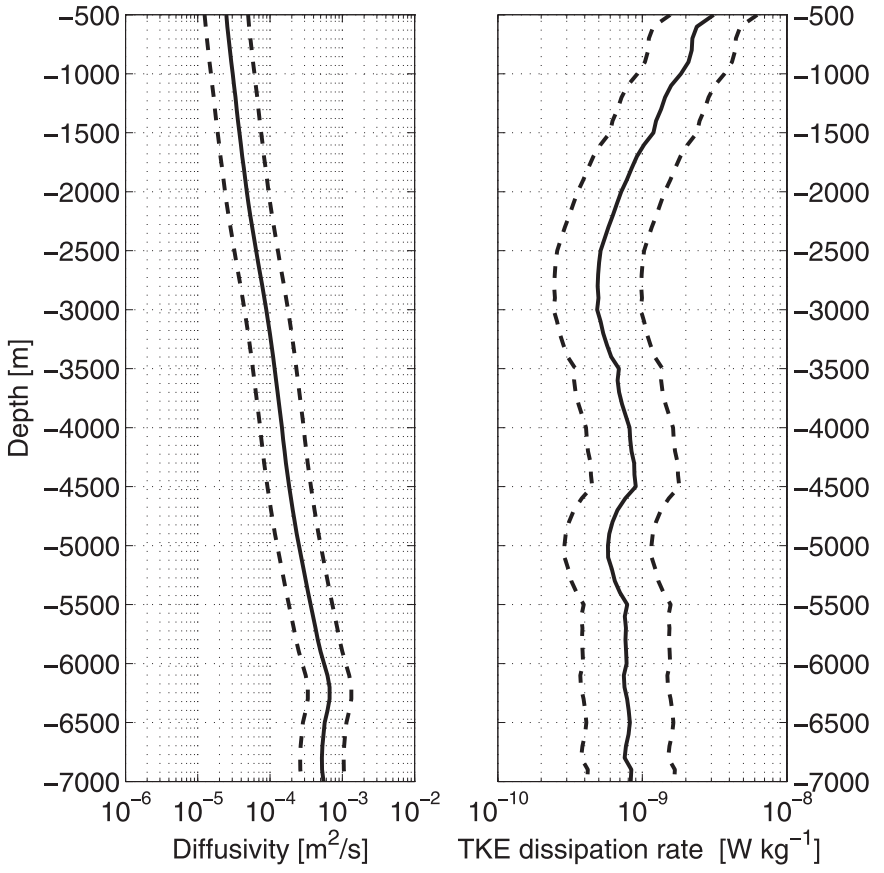

FIG. 11. Globally (40°S–48°N) averaged diapycnal diffusivity and TKE dissipation rates from the RDM. Dashed lines indicate a factor of 2 confidence range.

water conversion (O. A. Saenko 2009, personal communication). This supports the observations that a significant fraction of North Atlantic Deep Water (NADW) is converted to lighter water classes at the base of the pycnocline (e.g., Talley 2003) with the remaining conversion presumably occurring in the Southern Ocean.

Figure 11 shows the globally averaged (between 40°S and 48°N) diapycnal diffusivity profile and TKE dissipation rate profile as a function of depth. (The significance of the latitude boundaries will be made clear in a moment.) This is the global effective profile assuming that the products of locally enhanced mixing near rough topography are exported (via mesoscale and submesoscale circulation features) along neutral surfaces to the ocean interior away from the topography. The global effective diffusivity profile increases exponentially with depth until about 6200 m. It reaches the canonical value of 10^{-4} m^2 s^{-1} [required by Munk and Wunsch (1998) to maintain the stratification at depths between 1 and 4 km in the domain 40°S–48°N] only by a depth of about 3.2 km, but the profile does exceed 0.5×10^{-4} m^2 s^{-1} at all depths greater than about 2 km. It can be safely concluded, especially considering that the RDM errs on the conservative (smaller than observations) side, that topography-catalyzed diapycnal mixing is an important contributor to the maintenance of the abyssal stratification from the tropics to the midlatitudes. The globally averaged TKE dissipation rate profile decreases with depth, reaching a minimum of 5×10^{-10} W kg^{-1} at a depth of 3 km. At greater depths, the influence of bottom-enhanced mixing counteracts the effect of the decreasing stratification, resulting in a slight increase to about 10^{-9} W kg^{-1} at a depth of 4.5 km, below which the TKE dissipation rate remains approximately constant.

An alternative way of representing the global effective diffusivity is as a function of neutral density, allowing comparison with volume-averaged diffusivities estimated from inverse techniques (e.g., Ganachaud and Wunsch 2000; Lumpkin and Speer 2007). Figure 12 shows the volume-averaged diffusivity between neutral density layers delimiting equal ocean volumes between 32°S and 48°N as in Fig. 5 of Lumpkin and Speer (2007). Our diffusivity values for the same latitude range are quite similar for low densities but increase at a slower rate with neutral density than the volume-averaged diffusivities estimated by Lumpkin and Speer (2007). That the

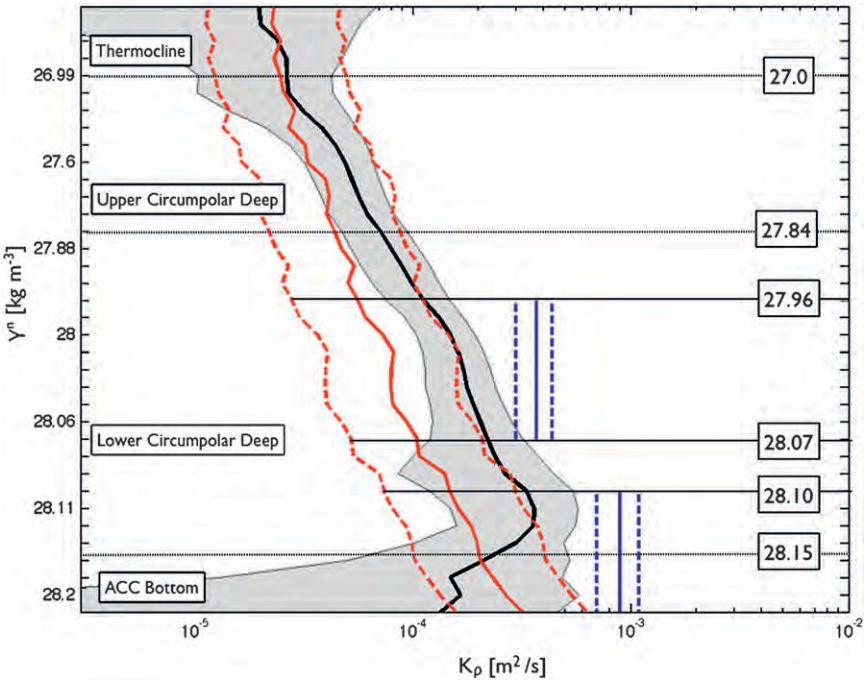

FIG. 12. Volume-averaged diapycnal diffusivity as a function of neutral density between 32°S and 48°N from Lumpkin and Speer (2007) (black line with standard error shaded) compared to predictions by the RDM (red line, dashed lines denote a factor of 2 confidence range). The nonlinear scale for neutral density is constructed such that each layer contains an equal ocean volume based on the Special Analysis Centre (SAC, Hamburg, Germany) climatology (Gouretski and Jancke 1998). Horizontal dashed lines denote approximate water mass divisions. The horizontal full lines denote the neutral density surfaces used in the analysis of Ganachaud and Wunsch (2000) for global deep ($27.96 < \gamma^n < 28.07$) and bottom ($\gamma^n > 28.10$) waters between 30°S and 48°N. Their volume-averaged diffusivity estimates are shown as vertical blue lines, with confidence intervals (dashed vertical blue lines) based on the output of a realistic numerical ocean model (Ganachaud 2003).

volume-averaged diffusivities predicted by the RDM for deep waters are lower than the estimates by Lumpkin and Speer (2007) may very well be due to the predicted vertical decay of the diffusivity being too fast for heights greater than 1500 m above the bottom, as discussed earlier. However, our estimates are nearly always within a factor of 2 of the Lumpkin and Speer (2007) estimates and certainly reproduce the same trend as a function of density.

In their earlier paper, Ganachaud and Wunsch (2000) estimated volume-averaged diffusivities for deep waters ($27.96 < \gamma^n < 28.07$ kg m^{-3}) and bottom waters ($\gamma^n > 28.10$ kg m^{-3}) between 30°S and 47°N, shown in blue in Fig. 12. The Ganachaud and Wunsch (2000) estimates also show an increase with neutral density but exceed the Lumpkin and Speer (2007) estimates. The difference between the two inversions may be due to a difference in the treatment of air–sea fluxes. Our estimates for these volumes, that is, 8.6×10^{-5} m^2 s^{-1} and 2.7×10^{-4} m^2 s^{-1}, respectively, are factors of 4 and 3 less than the Ganachaud and Wunsch (2000) estimates. Bearing in mind that while the collection of observed diffusivities used here is a large ensemble from multiple experiments, it remains a sparse sampling of the global ocean, and the differences with estimates from hydrographic inversions for deep and bottom waters may simply indicate that there are more intense mixing hot spots in the deep ocean that are not well represented in the microstructure surveys considered here, resulting in our estimates for the near-boundary diffusivities being too conservative. For instance, Ferron et al. (1998) inferred a mean diapycnal diffusivity of $\sim 10^{-1}$ m^2 s^{-1} for bottom waters in the Romanche Fracture Zone on the Mid-Atlantic Ridge based on the combination of fine structure data from CTD profiles, microstructure profiles, and a heat budget constructed from current meter data. More recently, MacKinnon et al. (2008) inferred a mean diapycnal diffusivity well in excess of 10^{-2} m^2 s^{-1} at several hundred meters from the bottom using Thorpe scale analysis and the Gregg–Henyey finescale parameterization applied to LADCP–CTD data in the Atlantis II fracture zone on the southwest Indian Ridge. The large mean diffusivities inferred in these fracture zones are orders of magnitude

TABLE 1. Volume estimates of the power consumed by diapycnal mixing under different scenarios for the spatial structure of the diapycnal diffusivity. The second column lists the power P consumed by mixing over various depth ranges for the global ocean (between 40°S and 48°N) estimated with the spatially variable $K_\rho(x, y, z)$ predicted by the RDM. The third column lists the averaged diffusivity over that ocean volume. The fourth column lists the power consumed assuming the diffusivity is constant within each volume and equal to that in column three. The difference in power consumption between columns 2 and 4 illustrates the bias toward higher power consumption estimates when the spatial variability of diffusivity is neglected. This is especially clear over large ocean volumes (i.e., 1–4- and 1–7-km depth ranges). The last column lists the power consumption estimates when the iconic diffusivity of 10^{-4} m^2 s^{-1} is used. All power consumption estimates here are computed with a spatially varying $N^2(x, y, z)$ derived from the 2005 *WOA* climatology.

Depth range (m)	$P[K_\rho(x, y, z)]$ (TW)	$\overline{K_\rho}$ (m^2 s^{-1})	$P(\overline{K_\rho})$ (TW)	$P(K_\rho = 10^{-4}$ m^2 s$^{-1})$ (TW)
500–1000	0.21	2.7×10^{-5}	0.22	0.90
1000–4000	0.37	7.0×10^{-5}	0.58	0.83
4000–7000	0.05	2.2×10^{-4}	0.05	0.02
1000–7000	0.42	9.5×10^{-5}	0.81	0.85

greater than the mean diffusivities observed in the microstructure surveys used for the construction of the RDM here.

Finally, the power consumed by the hypothesized mixing can be computed as

$$P = (1 + 1/\Gamma) \int \rho K_\rho(x, y, z) N^2(x, y, z)\, dV \qquad (5)$$

(e.g., St. Laurent and Simmons 2006). Munk and Wunsch (1998) made a rough estimate of the power consumed by mixing assuming a constant diffusivity of 10^{-4} m^2 s^{-1} over the abyssal ocean volume (1–4-km depth, 40°S–48°N). They further simplified Eq. (5) by assuming $\int N^2(x, y, z)\, dV \approx A \int N^2(z)\, dz \approx Ag\Delta\rho$, where A is the area of the ocean and g is the acceleration due to gravity. Taking the ocean area to be 3.6×10^{14} m^2 and the density difference $\Delta\rho$ between 1 and 4 km of depth as 1 kg m^{-3}, Munk and Wunsch (1998) found the now iconic value of $(1 + 1/\Gamma)Ag\Delta\rho \times 10^{-4} \approx 2.1$ TW to be consumed by mixing in the abyssal ocean. However, the value for the ocean area used (i.e., 3.6×10^{14} m^2) is actually the pole-to-pole area of the ocean at the surface. Using the more appropriate average ocean area between 1- and 4-km depth and between 40°S and 48°N, 2.35×10^{14} m^2 as estimated from SS97, reduces the 2.1-TW estimate to 1.4 TW. Furthermore, using $N^2(x, y, z)$ estimated from 2005 *WOA* data rather than the coarse approximation above reduces the 1.4-TW estimate to 0.83 TW (see Table 1). Evaluating (5) with the spatially varying diffusivity derived from our simple model, which unlike the Munk and Wunsch (1998) estimation does not produce a mean diffusivity as high as 10^{-4} m^2 s^{-1} except at depths below about 3200 m, further reduces the power consumption estimate to 0.37 TW. That is, the power consumed by our representation of the observed mixing in the abyssal ocean [defined, as in Munk and Wunsch (1998), as 1–4-km depth between 40°S and 48°N] is less than one-fifth of Munk and Wunsch's (1998) 2.1 TW. If we arbitrarily doubled the RDM estimates (per the crude factor of 2 confidence intervals employed above), so that our mean diffusivity in the abyssal ocean equaled or exceeded 10^{-4} m^2 s^{-1} below 2-km depth, the implied power consumption based on the RDM would still only be about a third of the canonical value.

A more recent estimate of power consumption was presented by St. Laurent and Simmons (2006). They divided the ocean between 30°S and 47°N into three volumes (bottom, deep, and ventilated) along neutral density surfaces as in Ganachaud and Wunsch (2000) and assigned a constant diffusivity value to each volume based on the inverse studies by Ganachaud and Wunsch (2000) and Lumpkin and Speer (2003). Their estimate of power consumption for the deep waters is 0.20–0.61 TW and for bottom water is 0.15–0.49 TW.

Power consumption estimates derived from the roughness diffusivity model for the same ocean volumes are 0.1 TW for the deep and 0.05 TW for the bottom waters, factors of 2–6 and 3–10 times smaller, respectively. We suspect a major factor in the discrepancy is the assumption of a constant diffusivity over large ocean volumes in St. Laurent and Simmons (2006). Estimates based on a constant, volume-averaged diffusivity quickly diverge from estimates based on a spatially variable diffusivity (e.g., cf. columns 2 and 4 in Table 1). In the case of bottom-intensified mixing, we generally find that $\int \rho \overline{K_\rho} N^2(x, y, z)\, dV \geq \int \rho K_\rho(x, y, z) N^2(x, y, z)\, dV$, where $\overline{K_\rho}$ is the volume-averaged $K_\rho(x, y, z)$. The dependence of power consumption on the spatial distribution of mixing and the lower values associated with nonuniform mixing are nothing new in the literature but perhaps merit more consideration. For instance, Simmons et al. (2004b) computed the power consumption (for the entire ocean depth) associated with (i) spatially variable mixing (specified by the JSL01 parameterization), (ii) mixing varying only in the vertical (based on the Bryan and Lewis (1979) profile), and (iii) uniform mixing. The globally averaged diffusivities for all three cases were kept the same but the power consumptions ranged from

1.01 TW (variable mixing) to 2.11 TW (varying only in the vertical) and to 5.80 TW (uniform mixing). Saenko (2006) also noted that the power consumed by two climate models having the same mean vertical profile of diffusivity but differing in their distributions (horizontally uniform versus topography intensified) is much greater in the case of the horizontally uniform mixing case. Considering that a large fraction of the power believed to be available for mixing the abyssal ocean is likely dissipated in the upper ocean {e.g., there are good reasons to suspect that much if not most of the 0.9 TW of open-ocean internal tide power is dissipated above 1 km [see, e.g., Althaus et al. (2003) and Klymak et al. (2006)]}, the more modest power consumption estimates associated with bottom-intensified mixing (such as the one provided here based on direct microstructure observations of abyssal turbulence) are more easily reconciled with current best estimates of the maximum power of ~2 TW available for mixing in the deep ocean (e.g., Wunsch and Ferrari 2004).

4. Conclusions

The principal objectives of this work are to contribute toward understanding the impacts of topography-catalyzed mixing on the distribution of water properties in the deep ocean and to improve mixing schemes for implementation into OGCMs. The vertical and horizontal variations of diapycnal mixing are believed to affect the structure of deep-ocean circulation (e.g., Hasumi and Suginohara 1999; Simmons et al. 2004b), so that incorporating a realistic distribution of diapycnal mixing into OGCMs can be expected to improve simulations of the MOC and its long-term variations. The work here, resulting in a roughness diffusivity model (RDM), differs from other published diffusivity parameterizations in that the RDM is based directly on fits to observations of turbulence in the deep ocean. The RDM also differs from other published diffusivity parameterizations [except Hasumi and Suginohara (1999) and Morris et al. (2001)] in that the bottom intensification of the diapycnal mixing is assumed to depend only on topographic roughness and height above bottom. While the latter may seem a step backward from the more physically based parameterizations of tidalgenic mixing that also take into account the spatially varying amplitudes of the barotropic tide currents, the aim here is to try to account for a broader range of mixing processes rather than just one component. Despite the broad range of possible energy sources and mixing processes contributing to topography-catalyzed mixing, the observed diffusivities were found to stratify according to a simple topographic roughness metric, suggesting that simple models such as the RDM will be useful until such time as specific dynamics-based parameterizations of all the important mixing processes are available. The parameters in the RDM describing the vertical decay of the bottom-intensified mixing were determined empirically from a large collection of microstructure data. The parameterization was then systematically extrapolated to investigate the potential impacts of such turbulence on global energy budgets and the maintenance of the abyssal stratification.

The microstructure-based diffusivity estimates revealed the following:

- a vertical decay of the mean K_ρ, with similar structure at all geographical locations, readily approximated by a power law decay as expected from Polzin's (2004) work, and
- a dependence of the maximum boundary diffusivity, K_b, and the diffusivity vertical scale height h_0, on topographic roughness [an attempt to determine a functional dependence of the vertical scale height on height above bottom, although anticipated from Polzin's (2004) work, was not successful with the available data].

The parameterization of K_ρ takes the functional form

$$K_\rho(h, r) = K_b(r)[1 + h/h_0(r)]^{-2} + K_{\text{back}}, \qquad (6)$$

where the boundary diffusivity $K_b(r)$ and the scale height $h_0(r)$ are simple functions of the seafloor roughness specified by Eqs. (3) and (4). Note that $K_b(r)$ and $h_0(r)$ are intimately tied to the choice of bathymetry (SS97) and roughness metric [Eq. (1)]; different choices for the bathymetry and roughness metric will alter the forms of these functions.

The RDM was shown to reproduce the mean diapycnal diffusivity structure derived from the microstructure observations to usually much better than a factor of 2 at nearly all heights up to 4500 m above the bottom at depths greater than 500 m (Fig. 9), which is an improvement over vertical structure functions with constant vertical decay scales used in current diffusivity parameterizations (Fig. 4). At heights greater than 1000 m above the bottom, the RDM vertical decay is slower than predicted by the JSL01 tide-based parameterization, resulting in a well-defined horizontal structure of RDM diffusivities at depths where JSL01 diffusvities have mostly decayed to near-background values (Fig. 11). Global maps of time mean ε and K_ρ predicted by the RDM show a spatial variation in the horizontal with similarities to the global dissipation and diffusivity maps based on tidal mixing parameterizations. However, notable regions of dissimilarity exist, such as at the East Pacific Rise, the Pacific–Antarctic Ridge, the mid–Indian Ridge and the southeast Indian Ridge. These regions are potential mixing hotspots

missed by tidal parameterizations. Whether they actually exhibit intensified mixing due to nontidal mixing phenomena will require further observations to verify.

Global volume-averaged diffusivities inferred from the RDM exhibit the same vertical structure patterns as those inferred from hydrographic data inversions, although our predictions are lower, suggesting perhaps that our maximum values of the boundary diffusivity are too conservative. Nevertheless, the correspondence supports the idea that water property distributions depend on processes that strongly mix the ocean at localized regions with the mixed products, but not the turbulence, advected laterally. Furthermore, the power consumption by bottom-intensified mixing in the abyssal ocean is found to be dependent on the spatial distribution of mixing. We here estimate that 0.37 TW are consumed by bottom-intensified mixing between 1- and 4-km depths, from 40°S to 48°N, considerably less than the now-canonical value of 2.1 TW presented by Munk and Wunsch (1998), and considerably more compatible with estimates of the power that is likely available for diapycnal mixing in the deep ocean. When applied to the global ocean from 72°S to 72°N (the coverage area of SS97), although this is not really appropriate in polar latitudes, the RDM predicts a power consumption of 0.45 TW between 1 and 4 km, and 0.51 TW between 1 km and the seafloor.

The RDM was based on microstructure data from tropical to midlatitudes. In the Arctic Ocean, energy sources for abyssal mixing are much weaker than at lower latitudes (e.g., Pinkel 2008). At high latitudes in the Southern Ocean, estimates of mixing based on finescale internal wave parameterizations applied to LADCP/CTD data suggest mixing to be intense throughout the entire water column (Polzin and Firing 1997; Garabato et al. 2004; Sloyan 2005), implying much larger decay scales than would be predicted by the RDM. The underlying causes for the different decay structures are unclear but may be due to the low stratification and/or difficulties in applying finescale parameterizations in a low stratification environment (Kunze et al. 2006). Given that the principal hypothesized energy source sustaining enhanced diapycnal mixing in the Southern Ocean is the instability of lee waves generated by flow over rough topography, it is possible that the strong, deep velocities of the Antarctic Circumpolar Current and their associated mesoscale eddies result in a decay structure unlike that observed at lower latitudes. Microstructure surveys would greatly help to elucidate the spatial structure of diapycnal mixing in the Southern Ocean.

Acknowledgments. We gratefully acknowledge Jody Klymak, Rick Lumpkin, Jim Moum, Alberto Naveira-Garabato, Thomas Sanford, and John Toole, who kindly and unhesitatingly shared their data. We thank G. Carter, C. Chavanne, E. Firing, P. Flament, M. Merrifield, and O. Saenko for helpful comments. This work was made possible by National Science Foundation Grants OCE98-19517 and OCE98-19533 that supported the HOME experiment.

REFERENCES

Alford, M. H., 2003: Improved global maps and 54-year history of wind-work on ocean inertial motions. *Geophys. Res. Lett.,* **30,** 1424, doi:10.1029/2002GL016614.

Althaus, A. M., E. Kunze, and T. B. Sanford, 2003: Internal tide radiation from Mendocino Escarpment. *J. Phys. Oceanogr.,* **33,** 1510–1527.

Armi, L., 1978: Some evidence for boundary mixing in the deep ocean. *J. Geophys. Res.,* **83** (C4), 1971–1979.

Aucan, J., and M. A. Merrifield, 2008: Boundary mixing associated with tidal and near-inertial internal waves. *J. Phys. Oceanogr.,* **38,** 1238–1252.

——, ——, D. S. Luther, and P. Flament, 2006: Tidal mixing events on the deep flanks of Kaena Ridge, Hawaii. *J. Phys. Oceanogr.,* **36,** 1202–1219.

Baker, M. A., and C. H. Gibson, 1987: Sampling turbulence in the stratified ocean—Statistical consequences of strong intermittency. *J. Phys. Oceanogr.,* **17,** 1817–1836.

Bell, T., 1975: Lee waves in stratified flows with simple harmonic time dependence. *J. Fluid Mech.,* **67,** 705–722.

Bray, N. A., and N. P. Fofonoff, 1981: Available potential energy for MODE eddies. *J. Phys. Oceanogr.,* **11,** 30–46.

Broersen, P., 2002: Automatic spectral analysis with time series models. *IEEE Trans. Instrum. Meas.,* **51,** 211–216.

Bryan, K., and L. Lewis, 1979: A water mass model of the world ocean. *J. Geophys. Res.,* **84** (C5), 2503–2517.

Carter, G. S., M. C. Gregg, and M. A. Merrifield, 2006: Flow and mixing around a small seamount on Kaena Ridge, Hawaii. *J. Phys. Oceanogr.,* **36,** 1036–1052.

De Szoeke, R. A., and A. F. Bennet, 1993: Microstructure fluxes across density surfaces. *J. Phys. Oceanogr.,* **23,** 2254–2264.

Dewar, W. K., R. J. Bingham, R. L. Iverson, D. P. Nowacek, L. C. St. Laurent, and P. H. Wiebe, 2006: Does the marine biosphere mix the ocean? *J. Mar. Res.,* **64,** 541–561.

Egbert, G. D., and R. D. Ray, 2001: Estimates of M-2 tidal energy dissipation from TOPEX/Poseidon altimeter data. *J. Geophys. Res.,* **106** (C10), 22 475–22 502.

——, and ——, 2003: Semi-diurnal and diurnal tidal dissipation from TOPEX/Poseidon altimetry. *Geophys. Res. Lett.,* **30,** 1907, doi:10.1029/2003GL017676.

Eriksen, C. C., 1998: Internal wave reflection and mixing at Fieberling Guyot. *J. Geophys. Res.,* **103** (C2), 2977–2994.

Ferron, B., H. Mercier, K. Speer, A. Gargett, and K. Polzin, 1998: Mixing in the Romanche Fracture Zone. *J. Phys. Oceanogr.,* **28,** 1929–1945.

Finnigan, T. D., D. S. Luther, and R. Lukas, 2002: Observations of enhanced diapycnal mixing near the Hawaiian ridge. *J. Phys. Oceanogr.,* **32,** 2988–3002.

Ganachaud, A., 2003: Error budget of inverse box models: The North Atlantic. *J. Atmos. Oceanic Technol.,* **20,** 1641–1655.

——, and C. Wunsch, 2000: Improved estimates of global ocean circulation, heat transport and mixing from hydrographic data. *Nature,* **408,** 453–457.

Garabato, A. C. N., K. L. Polzin, B. A. King, K. J. Heywood, and M. Visbeck, 2004: Widespread intense turbulent mixing in the Southern Ocean. *Science,* **303,** 210–213.

Garrett, C., and D. Gilbert, 1988: Estimates of vertical mixing by internal waves reflected of a sloping bottom. *Small-Scale Turbulence and Mixing in the Ocean,* J. Nihoul and B. Jamart, Eds., Elsevier, 405–424.

Gille, S. T., M. M. Yale, and D. T. Sandwell, 2000: Global correlation of mesoscale ocean variability with seafloor roughness from satellite altimetry. *Geophys. Res. Lett.,* **27,** 1251–1254.

Gouretski, V., and K. Jancke, 1998: A new climatology for the world ocean. WOCE Hydrographic Program Special Analysis Centre Tech. Rep. 3, 40 pp.

Gregg, M. C., 1987: Diapycnal mixing in the thermocline—A review. *J. Geophys. Res.,* **92** (C5), 5249–5286.

——, and T. B. Sanford, 1980: Signatures of mixing from the Bermuda Slope, the Sargasso Sea and the Gulf Stream. *J. Phys. Oceanogr.,* **10,** 105–127.

——, H. E. Seim, and D. B. Percival, 1993: Statistics of shear and turbulent dissipation profiles in random internal wave fields. *J. Phys. Oceanogr.,* **23,** 1777–1799.

——, T. B. Sanford, and D. P. Winkel, 2003: Reduced mixing from the breaking of internal waves in equatorial waters. *Nature,* **422,** 513–515.

Hasumi, H., and N. Suginohara, 1999: Effects of locally enhanced vertical diffusivity over rough bathymetry on the world ocean circulation. *J. Geophys. Res.,* **104** (C10), 23 367–23 374.

Henyey, F., J. Wright, and S. Flatte, 1986: Energy and action flow through the internal wave field: An eikonal approach. *J. Geophys. Res.,* **91** (C7), 9686–9698.

Hibiya, T., M. Nagasawa, and Y. Niwa, 2006: Global mapping of diapycnal diffusivity in the deep ocean based on the results of expendable current profiler (XCP) surveys. *Geophys. Res. Lett.,* **33,** L03611, doi:10.1029/2005GL025218.

Huang, R. X., and X. Z. Jin, 2002: Deep circulation in the South Atlantic induced by bottom-intensified mixing over the midocean ridge. *J. Phys. Oceanogr.,* **32,** 1150–1164.

Ivey, G. N., 1987: The role of boundary mixing in the deep ocean. *J. Geophys. Res.,* **92** (C11), 11 873–11 878.

Jayne, S. R., 2009: The impact of abyssal mixing parameterizations in an ocean general circulation model. *J. Phys. Oceanogr.,* **39,** 1756–1775.

——, and L. C. St. Laurent, 2001: Parameterizing tidal dissipation over rough topography. *Geophys. Res. Lett.,* **28,** 811–814.

——, ——, and S. Gille, 2004: Connections between ocean bottom topography and Earth's climate. *Oceanography,* **17,** 65–74.

Katsman, C. A., 2006: Impacts of localized mixing and topography on the stationary abyssal circulation. *J. Phys. Oceanogr.,* **36,** 1660–1671.

Klymak, J. M., and Coauthors, 2006: An estimate of tidal energy lost to turbulence at the Hawaiian Ridge. *J. Phys. Oceanogr.,* **36,** 1148–1164.

——, R. Pinkel, and L. Rainville, 2008: Direct breaking of the internal tide near topography: Kaena Ridge. *J. Phys. Oceanogr.,* **38,** 380–399.

Koch-Larrouy, A., G. Madec, P. Bouruet-Aubertot, T. Gerkema, L. Bessieres, and R. Molcard, 2007: On the transformation of Pacific Water into Indonesian Throughflow Water by internal tidal mixing. *Geophys. Res. Lett.,* **34,** L04604, doi:10.1029/2006GL028405.

Kuhlbrodt, T., A. Griesel, M. Montoya, A. Levermann, M. Hofmann, and S. Rahmstorf, 2007: On the driving processes of the Atlantic meridional overturning circulation. *Rev. Geophys.,* **45,** RG2001, doi:10.1029/2004RG000166.

Kunze, E., and T. B. Sanford, 1996: Abyssal mixing: Where it is not. *J. Phys. Oceanogr.,* **26,** 2286–2296.

——, and J. M. Toole, 1997: Tidally driven vorticity, diurnal shear, and turbulence atop Fieberling Seamount. *J. Phys. Oceanogr.,* **27,** 2663–2693.

——, E. Firing, J. M. Hummon, T. K. Chereskin, and A. M. Thurnherr, 2006: Global abyssal mixing inferred from lowered ADCP shear and CTD strain profiles. *J. Phys. Oceanogr.,* **36,** 1553–1576.

Ledwell, J. R., E. T. Montgomery, K. L. Polzin, L. C. St. Laurent, R. W. Schmitt, and J. M. Toole, 2000: Evidence for enhanced mixing over rough topography in the abyssal ocean. *Nature,* **403,** 179–182.

Lee, C., E. Kunze, T. B. Sanford, J. D. Nash, M. A. Merrifield, and P. E. Holloway, 2006: Internal tides and turbulence along the 3000-m isobath of the Hawaiian Ridge. *J. Phys. Oceanogr.,* **36,** 1166–1183.

Legg, S., 2003: Internal wave breaking at variable topographic slopes. *Near-Boundary Processes and Their Parameterization: Proc. 13th 'Aha Huliko'a Hawaiian Winter Workshop,* Honolulu, HI, University of Hawaii at Manoa, 69–72. [Available online at http://www.soest.hawaii.edu/PubServices/2003pdfs/Legg.pdf.]

Levine, M. D., and T. J. Boyd, 2006: Tidally forced internal waves and overturns observed on a slope: Results from HOME. *J. Phys. Oceanogr.,* **36,** 1184–1201.

Lozovatsky, I. D., H. J. S. Fernando, and S. M. Shapolav, 2008: Deep-ocean mixing on the basin scale: Inference from North-Atlantic studies. *Deep-Sea Res. I,* **55,** 1075–1089.

Lueck, R., and R. Reid, 1984: On the production and dissipation of mechanical energy in the ocean. *J. Geophys. Res.,* **89** (C3), 3439–3445.

Lukas, R., F. Santiago-Mandujano, F. Bingham, and A. Mantyla, 2001: Cold bottom water events observed in the Hawaii ocean time series: Implications for vertical mixing. *Deep-Sea Res. I,* **48,** 995–1021.

Lumpkin, R., and K. Speer, 2003: Large-scale vertical and horizontal circulation in the North Atlantic Ocean. *J. Phys. Oceanogr.,* **33,** 1902–1920.

——, and ——, 2007: Global ocean meridional overturning. *J. Phys. Oceanogr.,* **37,** 2550–2562.

Mackinnon, J. A., and K. B. Winters, 2003: Spectral evolution of bottom-forced internal waves. *Near-Boundary Processes and Their Parameterization: Proc. 13th 'Aha Huliko'a Hawaiian Winter Workshop,* Honolulu, HI, University of Hawaii at Manoa, 73–83. [Available online at http://www.soest.hawaii.edu/PubServices/2003pdfs/Mackinnon.pdf.]

——, T. M. S. Johnston, and R. Pinkel, 2008: Strong transport and mixing of deep water through the southwest Indian Ridge. *Nature Geosci.,* **1,** 755–758.

Marshall, D. P., and A. C. Naveira Garabato, 2008: A conjecture on the role of bottom-enhanced diapycnal mixing in the parameterization of geostrophic eddies. *J. Phys. Oceanogr.,* **38,** 1607–1613.

Martin, J. P., and D. L. Rudnick, 2007: Inferences and observations of turbulent dissipation and mixing in the upper ocean at the Hawaiian Ridge. *J. Phys. Oceanogr.,* **37,** 476–494.

——, ——, and R. Pinkel, 2006: Spatially broad observations of internal waves in the upper ocean at the Hawaiian Ridge. *J. Phys. Oceanogr.,* **36,** 1085–1103.

McComas, C. H., and P. Müller, 1981: The dynamic balance of internal waves. *J. Phys. Oceanogr.,* **11,** 970–986.

McDougall, T. J., 1991: Parameterizing mixing in inverse models. *Dynamics of Oceanic Internal Gravity Waves: Proc. 'Aha Huliko'a Hawaiian Winter Workshop,* Honolulu, HI, University of Hawaii

at Manoa, 355–386. [Available online at http://www.soest.hawaii.edu/PubServices/1991pdfs/McDougall.pdf.]

Merrifield, M. A., and P. E. Holloway, 2002: Model estimates of M2 internal tide energetics at the Hawaiian Ridge. *J. Geophys. Res.,* **107,** 3179, doi:10.1029/2001JC000996.

Montgomery, E. T., 1998: Use of the High Resolution Profiler (HRP) in the Brazil Basin Tracer Release Experiment. Woods Hole Oceanographic Institution Tech. Rep. 98-08, 38 pp.

——, and J. M. Toole, 1993: Fine- and microstructure observations at Fieberling Guyot. R/V New Horizon cruise report. Woods Hole Oceanographic Institution Tech. Rep. 93-51, 27 pp.

Morris, M. Y., M. M. Hall, L. C. St. Laurent, and N. G. Hogg, 2001: Abyssal mixing in the Brazil Basin. *J. Phys. Oceanogr.,* **31,** 3331–3348.

Müller, P., and N. Xu, 1992: Scattering of oceanic internal gravity-waves off random bottom topography. *J. Phys. Oceanogr.,* **22,** 474–488.

Munk, W., 1966: Abyssal recipes. *Deep-Sea Res. I,* **13,** 207–230.

——, and C. Wunsch, 1998: Abyssal recipes II: Energetics of tidal and wind mixing. *Deep-Sea Res. I,* **45,** 1977–2010.

Nash, J. D., E. Kunze, J. M. Toole, and R. W. Schmitt, 2004: Internal tide reflection and turbulent mixing on the continental slope. *J. Phys. Oceanogr.,* **34,** 1117–1134.

Oakey, N. S., 1982: Determination of the rate of dissipation of turbulent energy from simultaneous temperature and velocity shear microstructure measurements. *J. Phys. Oceanogr.,* **12,** 256–271.

Osborn, T. R., 1980: Estimates of the local-rate of vertical diffusion from dissipation measurements. *J. Phys. Oceanogr.,* **10,** 83–89.

Pinkel, R., 2008: The wavenumber-frequency spectrum of vortical and internal-wave shear in the western Arctic Ocean. *J. Phys. Oceanogr.,* **38,** 277–290.

Polzin, K., 1992: Observations of turbulence, internal waves and background flows: An inquiry into relationships between scales of motion. Ph.D. dissertation, MIT–WHOI Joint Program in Oceanography, WHOI Tech. Rep. WHOI-92-39, 244 pp.

——, 1999: A rough recipe for the energy balance of quasi-steady internal lee waves. *Dynamics of Oceanic Internal Gravity Waves, II: 'Aha Huliko'a Hawaiian Winter Workshop,* Honolulu, HI, University of Hawaii at Manoa, 117–128. [Available online at http://www.soest.hawaii.edu/PubServices/1999pdfs/Polzin.pdf.]

——, 2004: Idealized solutions for the energy balance of the finescale internal wave field. *J. Phys. Oceanogr.,* **34,** 231–246.

——, 2009: An abyssal recipe. *Ocean Modell.,* **30** (4), 298–309.

——, and E. Firing, 1997: Estimates of diapycnal mixing using LADCP and CTD data from I8S. International WOCE Newsletter, No. 29, WOCE International Project Office, Southampton, United Kingdom, 39–42.

——, J. M. Toole, and R. W. Schmitt, 1995: Finescale parameterizations of turbulent dissipation. *J. Phys. Oceanogr.,* **25,** 306–328.

——, ——, J. R. Ledwell, and R. W. Schmitt, 1997: Spatial variability of turbulent mixing in the abyssal ocean. *Science,* **276,** 93–96.

Rainville, L., and R. Pinkel, 2006a: Baroclinic energy flux at the Hawaiian Ridge: Observations from the R/P *FLIP*. *J. Phys. Oceanogr.,* **36,** 1104–1122.

——, and ——, 2006b: Propagation of low-mode internal waves through the ocean. *J. Phys. Oceanogr.,* **36,** 1220–1236.

Rudnick, D. L., and Coauthors, 2003: From tides to mixing along the Hawaiian ridge. *Science,* **301,** 355–357.

Saenko, O. A., 2006: The effect of localized mixing on the ocean circulation and time-dependent climate change. *J. Phys. Oceanogr.,* **36,** 140–160.

——, 2008: On the strong seasonal currents in the deep ocean. *J. Climate,* **21,** 5642–5656.

——, and W. J. Merryfield, 2005: On the effect of topographically enhanced mixing on the global ocean circulation. *J. Phys. Oceanogr.,* **35,** 826–834.

Samelson, R. M., 1998: Large-scale circulation with locally enhanced vertical mixing. *J. Phys. Oceanogr.,* **28,** 712–726.

Seber, G. A. F., and C. J. Wild, 1989: *Nonlinear Regression*. John Wiley and Sons, 768 pp.

Simmons, H. L., R. W. Hallberg, and B. K. Arbic, 2004a: Internal wave generation in a global baroclinic tide model. *Deep-Sea Res. II,* **51,** 3043–3068.

——, S. R. Jayne, L. C. St. Laurent, and A. J. Weaver, 2004b: Tidally driven mixing in a numerical model of the ocean general circulation. *Ocean Modell.,* **6,** 245–263.

Sloyan, B. M., 2005: Spatial variability of mixing in the Southern Ocean. *Geophys. Res. Lett.,* **32,** L18603, doi:10.1029/2005GL023568.

Smith, W. H. F., and D. T. Sandwell, 1997: Global sea floor topography from satellite altimetry and ship depth soundings. *Science,* **277,** 1956–1962.

St. Laurent, L., 1999: Diapycnal advection by double diffusion and turbulence in the ocean. Ph.D dissertation, MIT–WHOI Joint Program in Oceanography, 139 pp.

——, and J. D. Nash, 2003: Internal tide energy dissipated near topography. *Near-Boundary Processes and Their Parameterization: Proc. 13th 'Aha Huliko'a Hawaiian Winter Workshop,* Honolulu, HI, University of Hawaii at Manoa, 45–58. [Available online at http://www.soest.hawaii.edu/PubServices/2003pdfs/Stlaurent.pdf.]

——, and H. Simmons, 2006: Estimates of power consumed by mixing in the ocean interior. *J. Climate,* **19,** 4877–4890.

——, J. M. Toole, and R. W. Schmitt, 2001: Buoyancy forcing by turbulence above rough topography in the abyssal Brazil Basin. *J. Phys. Oceanogr.,* **31,** 3476–3495.

——, H. L. Simmons, and S. R. Jayne, 2002: Estimating tidally driven mixing in the deep ocean. *Geophys. Res. Lett.,* **29,** 2106, doi:10.1029/2002GL015633.

Talley, L. D., 2003: Shallow, intermediate and deep overturning components of the global heat budget. *J. Phys. Oceanogr.,* **33,** 530–560.

Thurnherr, A. M., L. C. St. Laurent, K. G. Speer, J. M. Toole, and J. R. Ledwell, 2005: Mixing associated with sills in a canyon on the midocean ridge flank. *J. Phys. Oceanogr.,* **35,** 1370–1381.

Toole, J. M., 1998: Turbulent mixing in the ocean. *Ocean Modeling and Parameterization,* E. P. Chassignet and J. Veron, Eds., NATO Science Series C, Vol. 516, 171–187.

——, 2007: Temporal characteristics of abyssal finescale motions above rough bathymetry. *J. Phys. Oceanogr.,* **37,** 409–427.

——, R. W. Schmitt, K. L. Polzin, and E. Kunze, 1997: Near-boundary mixing above the flanks of a midlatitude seamount. *J. Geophys. Res.,* **102** (C1), 947–959.

Williams, P. D., T. W. Haine, and P. L. Read, 2008: Inertia–gravity waves emitted from balanced flow: Observations, properties, and consequences. *J. Atmos. Sci.,* **65,** 3543–3556.

Wunsch, C., and R. Ferrari, 2004: Vertical mixing, energy and the general circulation of the oceans. *Annu. Rev. Fluid Mech.,* **36,** 281–314.

Zaron, E. D., and G. D. Egbert, 2006: Estimating open-ocean barotropic tidal dissipation: The Hawaiian Ridge. *J. Phys. Oceanogr.,* **36,** 1019–1035.

Zhang, J. B., R. W. Schmidt, and R. X. Huang, 1999: The relative influence of diapycnal mixing and hydrologic forcing on the stability of the thermohaline circulation. *J. Phys. Oceanogr.,* **29,** 1096–1108.